

The Simulated Catalogue of Optical Transients and Correlated Hosts (SCOTCH)

Martine Lokken^{1,2,3*}, Alexander Gagliano^{4,5,6†}, Gautham Narayan^{4,5}, Renée Hložek^{1,3}, Richard Kessler^{7,8}, John Franklin Crenshaw⁹, Laura Salo¹⁰, Catarina S. Alves¹¹, Deep Chatterjee^{4,5}, Maria Vincenzi¹², Alex I. Malz^{13,14}, The LSST Dark Energy Science Collaboration

¹David A. Dunlap Department of Astronomy and Astrophysics, University of Toronto, 50 St. George Street, Toronto, Ontario, M5S 3H4 Canada

²Canadian Institute for Theoretical Astrophysics, University of Toronto, 60 St. George St., Toronto, ON M5S 3H4, Canada

³Dunlap Institute of Astronomy & Astrophysics, 50 St. George St., Toronto, ON M5S 3H4, Canada

⁴Department of Astronomy, University of Illinois at Urbana-Champaign, 1002 W. Green St., IL 61801, USA

⁵Center for Astrophysical Surveys, National Center for Supercomputing Applications, Urbana, IL, 61801, USA

⁶National Science Foundation Graduate Research Fellow

⁷Department of Astronomy and Astrophysics, University of Chicago, Chicago, IL 60637, USA

⁸Kavli Institute for Cosmological Physics, University of Chicago, Chicago, IL 60637, USA

⁹DIRAC Institute and Department of Physics, University of Washington, Seattle, WA 98195, USA

¹⁰School of Physics and Astronomy, University of Minnesota, 116 Church Street S.E., Minneapolis, MN 55455, USA

¹¹Department of Physics & Astronomy, University College London, Gower Street, London WC1E 6BT, UK

¹²Department of Physics, Duke University Durham, NC 27708, USA

¹³Ruhr-University Bochum, German Centre for Cosmological Lensing, Universitätsstraße 150, 44801 Bochum, Germany

¹⁴McWilliams Center for Cosmology, Department of Physics, Carnegie Mellon University

Accepted XXX. Received YYY; in original form ZZZ

ABSTRACT

As we observe a rapidly growing number of astrophysical transients, we learn more about the diverse host galaxy environments in which they occur. Host galaxy information can be used to purify samples of cosmological Type Ia supernovae, uncover the progenitor systems of individual classes, and facilitate low-latency follow-up of rare and peculiar explosions. In this work, we develop a novel data-driven methodology to simulate the time-domain sky that includes detailed modeling of the probability density function for multiple transient classes conditioned on host galaxy magnitudes, colours, star formation rates, and masses. We have designed these simulations to optimize photometric classification and analysis in upcoming large synoptic surveys. We integrate host galaxy information into the SNANA simulation framework to construct the Simulated Catalogue of Optical Transients and Correlated Hosts (SCOTCH), a publicly-available catalogue of 5 million idealized transient light curves in LSST passbands and their host galaxy properties over the redshift range $0 < z < 3$. This catalogue includes supernovae, tidal disruption events, kilonovae, and active galactic nuclei. Each light curve consists of true top-of-the-galaxy magnitudes sampled with high ($\lesssim 2$ day) cadence. In conjunction with SCOTCH, we also release an associated set of tutorials and the transient-specific libraries to enable simulations of arbitrary space- and ground-based surveys. Our methodology is being used to test critical science infrastructure in advance of surveys by the Vera C. Rubin Observatory and the Nancy G. Roman Space Telescope.

Key words: transients: supernovae – software: simulations – catalogues

1 INTRODUCTION

An era of rapid and large-scale astrophysical data collection is underway. Surveys are now detecting transient events across large swaths of the sky, e.g. the Zwicky Transient Facility (ZTF; Bellm et al. 2019), ASAS-SN (Shappee et al. 2014), Gaia (Gaia Collaboration et al. 2016), and MeerKAT (Jonas 2009). Entirely novel classes of events, including those at higher redshifts, will soon be revealed as telescopes such as the Vera C. Rubin Observatory (Ivezić et al. 2019), the Nancy Grace Roman Space Telescope (Spergel et al. 2015), and

the James Webb Space Telescope (Gardner et al. 2006) begin collecting data. Notable among these, the Rubin Observatory (set to begin science operations in Chile in 2024) will undertake the Legacy Survey of Space and Time (LSST), expected to observe millions of transients out to and beyond $z \sim 1$ as it repeatedly scans 18,000 square degrees of the sky.

The science goals of these large-scale transient surveys are manifold, but include measuring the expansion history of the universe, improving our understanding of progenitor physics, and discovering faster and fainter transients that have eluded prior searches. Accurate classification will be paramount for each of these goals. In the majority of cases, transients discovered in upcoming surveys must be classified without spectroscopic information. Algorithms that clas-

* E-mail: m.lokken@mail.utoronto.ca

† E-mail: gaglian2@illinois.edu

sify transients based on photometry alone have proliferated in recent years, some based on traditional template-matching methods and others employing novel machine learning algorithms (e.g., Villar et al. 2020; Möller & de Boissière 2020; Qu et al. 2021; Alves et al. 2022).

Multiple studies have demonstrated correlations between the class of a transient and the properties of the galaxy where it occurs (deemed its “host galaxy”). Where light curve sampling is sparse, host galaxy data can be used to more easily distinguish transients of different classes. The occurrence rate of Type Ia supernovae (SNe Ia) is directly proportional to both the stellar mass and the star formation rate of its host galaxy, although a non-negligible subset has also been discovered in passive galaxies (Sullivan et al. 2006). As the end-states of short-lived (~ 50 Myr) massive stars, Core-Collapse SNe (CCSNe) are most likely to occur in spiral galaxies undergoing periods of significant star formation (Svensson et al. 2010). Variations also arise in the host populations of stripped-envelope SNe, events characterized by a dearth of hydrogen (SNe Ib) and helium (SNe Ic) in spectral observations. Broad-lined SNe Ic (SNe Ic-BL), the only supernovae to be unambiguously associated with long-duration Gamma Ray Bursts (LGRBs; Japelj et al. 2016), have host galaxies with lower average metallicity than their less-energetic counterparts (SNe Ic; Modjaz et al. 2020). This suggests a potential relationship between progenitor metallicity and the formation of jets during stellar death (Graham & Fruchter 2013). Further, SED fits to multi-band photometry of Type-I (Hydrogen-poor) Super-Luminous SN (SLSN-I) hosts have revealed that these events occur almost exclusively in metal-poor, low-mass, star-forming host galaxies (Leloudas et al. 2015; Perley et al. 2016; Angus et al. 2016). In the pursuit of optimally-standardized light curves for cosmology, subtler correlations between SN Ia photometry and host galaxy mass and star formation rate have also been identified (Lampeitl et al. 2010; Sullivan et al. 2010; Barkhudaryan et al. 2019; Rose et al. 2019; Brout & Scolnic 2021).

At low redshifts, spatially resolved studies enabled by multi-wavelength photometry and Integral Field Unit spectroscopy have revealed additional local-scale correlations. From a sample of 519 host galaxies selected in the Sloan Digital Sky Survey (SDSS; Blanton et al. 2017), Kelly & Kirshner (2012) found that SNe Ic-BL and SNe Ib occurred in extremely blue locations. Local correlations are weak for SNe Ia (Anderson et al. 2015): due to the advanced ages of their white-dwarf progenitors (\sim Gyrs), these systems can migrate substantially from formation to explosion. Nevertheless, the environment may alter the evolution of an event for the same progenitor. Spatially-resolved host galaxy information can also be used to distinguish between SN explosion models in the absence of direct detections of a progenitor (Raskin et al. 2008; Fruchter et al. 2006). Preliminary correlations have been identified in recent years for rare classes of events, including a preference of Rapidly-Evolving Transients (RETs; Drout et al. 2014; Pursiainen et al. 2018) for hosts of intermediate mass between high-mass SN Ia hosts and low-mass SLSN hosts (Wiseman et al. 2020). For observationally rare events (e.g., kilonovae; Smartt et al. 2017), correlations remain as yet unconstrained, but may play a decisive role in maximizing the yield of future targeted searches. Upcoming surveys are well-poised to further extend our understanding of these class-specific correlations toward higher redshifts and rare sub-types. However, only a few transient classifiers to date (Foley & Mandel 2013; Gagliano et al. 2021) have incorporated host galaxy information. Efforts are stymied by the limited observational data available for training these algorithms; perhaps worse, extant samples are frequently biased toward low-redshift, bright host galaxies, uncharacteristic of the galaxies anticipated from upcoming surveys. Where sample sizes are small,

more common classes can act as a surrogate in training sets, if the physical environments are expected to be similar.

In this transitional period when observed transient samples are limited to the local universe, simulations are vital for developing and testing classification algorithms that incorporate host galaxy information. To further enable these efforts, we present the first large-scale simulation of optical transients *and their host galaxies* that extrapolates existing data to high redshifts ($z \sim 3$). This work extends the simulations generated for the Photometric LSST Astronomical Time-Series Classification Challenge (PLAsTiCC; Kessler et al. 2019). PLAsTiCC data were generated by simulation code in the SuperNova ANalysis package (Kessler et al. 2009, SNANA), and the challenge represented the first large-scale effort to realistically simulate a wide range of transients. Simulated host-galaxy information, however, was limited: the dataset only includes the photometric redshifts of host galaxies assigned near the redshift of the transient. This work extends the PLAsTiCC framework with the inclusion of empirical and theoretical host-galaxy correlations for both common and rare transient classes. We embed these correlations using a series of host galaxy libraries (called HOSTLIBS within SNANA) and weight maps (WGTMAPS) that describe the likelihood of a given galaxy to host a certain class of transient within the simulation.

Our work is enabled by multiple previous efforts to consolidate the properties of transient host galaxy populations. The GRB Host Studies catalogue¹ (GHoST; Savaglio et al. 2006a) consolidates derived host galaxy information (including star formation rate, stellar mass, and redshift) for ~ 100 gamma-ray bursts (GRBs), finding that these bursts occur preferentially in star-forming, low-mass galaxies. Gagliano et al. (2021) constructed the Galaxies Hosting Supernovae and other Transients (GHOST) Catalogue, which contains the optical photometric properties of $\sim 16,500$ galaxies that have hosted observed SNe of all classes. At the time of writing, Qin et al. (2022) has released the Transient Host Exchange (THEX), a catalogue containing $> 36,000$ host galaxies of many transient types and the photometric properties of their hosts spanning infrared to ultraviolet wavelengths.

There is precedent to the use of host galaxy libraries in supernova simulations. In SNANA, HOSTLIBS were first used to model Poisson noise in simulated bias corrections for SN Ia distances for the Joint Lightcurve Analysis (Kessler et al. 2013; Betoule et al. 2014). HOSTLIBS were similarly used to forecast constraints for the Nancy Grace Roman Space Telescope (Hounsell et al. 2018). The Pantheon (Scolnic et al. 2018) and DES 3-year (Abbott et al. 2019; Brout et al. 2019) SN Ia-cosmology analyses further extended the scope of these files to account for correlations between SN properties and host galaxy stellar mass. An alternative machine learning-based simulation, EmpiriciSN (Holoien et al. 2017), employed a library of photometric host galaxy data in SDSS to generate synthetic light curves of SNe Ia.

As part of the recent Dark Energy Survey (DES) cosmology analysis using photometrically-identified SNe Ia, Vincenzi et al. (2021) expanded the SNANA-specific HOSTLIB framework to realistically simulate SN host galaxies by class using a set of physically-motivated WGTMAP files. To account for contamination from non-Ia classes, their simulation includes core-collapse SNe (CC SNe, including II and Ib/c) and considers the dependence on host galaxy mass and star formation rate for each SN type. The resulting SN Ia+CC SN simulation of host properties and SN-host correlations shows excellent

¹ <http://www.grbhosts.org/>

agreement with DES data, and this simulation is now in use as a training set for photometric classifiers (Möller 2022, *in prep.*).

In this work, we extend the results of Vincenzi et al. (2021) by simulating additional supernovae and other non-SN transients, incorporating correlations with hosts across a wider range of properties, and separately validating hosts of different classes across these properties. We extrapolate information from archival events, mostly at low-redshift, to a high-redshift simulated sample of galaxies via associations in intrinsic—rather than observed—properties. In doing so, we encode correlations for each transient class to significantly higher redshifts ($z \sim 3$) than the ranges spanned by currently-available observations. SCOTCH² can be used to test classifier algorithms and alert broker systems, examine the effects of contamination on cosmological analyses, and model selection biases in current and upcoming transient/host galaxy surveys.

Our paper is outlined as follows. We introduce the archival catalogues used to construct our host galaxy sample in §3, and describe the SNANA simulation code that we use to generate our transient events and summarize the models underlying each event in §4. Our methodology is presented in §5 for combining observed and simulated catalogues into a library containing millions of host galaxies. We then describe our process for incorporating additional class-specific transient correlations using WGTMAPs in §6. We validate our results in §7 and present the schema of our final catalogue in §8. We conclude with a discussion of the limitations of our sample and areas for future research in §9.

2 METHODOLOGY OVERVIEW

Because the methods we use to simulate the transients themselves are nearly identical to those described in Kessler et al. (2019), this paper focuses on our methodology for constructing a set of HOSTLIBS and WGTMAPs for the SNANA simulation code. This allows us to realistically associate a simulated host galaxy with each transient, given its class. We provide a flowchart of this pipeline in Fig. 1. The initial input is the CosmoDC2 synthetic galaxy catalogue (Korytov et al. 2019, described in §3.1) with slight modifications made via the PZFLow algorithm (Crenshaw et al. 2021, described in §5.2). First, we create three large libraries of galaxies by selecting synthetic galaxies matching the rest-frame colour and absolute magnitude distributions of three broad categories of transient hosts in observational data. We utilize the observational data in GHOST (Gagliano et al. 2021), a catalogue of supernova host galaxy properties described in additional detail in §3.2. Our process for selecting synthetic galaxies matching the observational data, including the use of the ANNOY³ algorithm, are described in detail in §5.3. The resulting galaxy libraries include: Type Ia hosts (I); Type II, II_n, II_p hosts (II); and Type Ib, Ic, II_b hosts (III). We construct an additional library of randomly-selected CosmoDC2 galaxies to serve as the hosts of transients from classes that have little observational data, and for which the correlation between explosion and environment is unconstrained by GHOST. Next, for nine different transient classes, we encode the probability that an event of that class will occur in a host galaxy given its mass and star formation rate. The probabilities are described in §6. Finally, the SNANA simulation (§4) is used to generate transient light curves, place each in a realistically-associated host galaxy, and model instrumental noise. In this final stage, host galaxies are selected from one of the

four libraries depending on the transient class, with the probability of selection given by the class-specific functions described in §6.

3 GALAXY DATA

3.1 The DC2 Simulations

Our work aims to simulate transient-host associations to higher redshifts and fainter magnitudes than have been previously observed. We also wish to produce a catalogue containing valuable derived properties of transient hosts, including photometry, morphology, star formation rates and stellar masses. Existing galaxy catalogues are limited in these respects, so we make use of synthetic galaxy data from the LSST Dark Energy Science Collaboration (DESC).

DESC is in the midst of a series of data challenges in preparation for the Rubin Observatory. The goal of the data challenges is to produce realistic end-to-end simulations of LSST survey operations, data reduction, and analysis. For data challenge 2 (DC2), DESC produced a suite of simulated LSST-like datasets including an extragalactic source catalogue and co-added images (LSST Dark Energy Science Collaboration et al. 2021). We make use of the extragalactic catalogue, named the CosmoDC2 Synthetic Sky catalogue (Korytov et al. 2019), and its associated DC2 image data.

The CosmoDC2 catalogue was constructed from a dark matter only N-body simulation in a 4.225 Gpc³ volume, where realistic galaxies with Sersic profiles and SEDs were associated with dark matter halos. The resultant galaxy catalogue, which is delivered in HEALPix⁴ (Hierarchical Equal Area iso-Latitude Pixelization) format (Górski et al. 2005), spans 440 deg² of the sky and cosmological distances ($z \simeq 3$). The CosmoDC2 data has also undergone rigorous validation to ensure that it matches observed galaxy properties (Kovacs et al. 2021). However, due to necessary compromises made to accommodate the needs of the diverse DESC working groups, the CosmoDC2 distributions of galaxy colors are far from perfect, particularly at higher redshifts ($z > .5$). We discuss how these colour limitations affect the final SCOTCH catalogue in §7.

We use the GRCatalogs⁵ analysis tool (Mao et al. 2018) to select CosmoDC2 galaxies within 31 neighbouring HEALPixels. The selected HEALPixels are chosen to completely overlap with the DC2 image catalogues (LSST Dark Energy Science Collaboration (LSST DESC) et al. 2021), which contain image properties for CosmoDC2 galaxies as LSST would observe them over 5 years, extending to $r = 28$. The overlap in coverage between these HEALPixels and the image catalogue is shown in Fig. 2. To ensure the generality of our final catalogue, the sky coverage displayed in the figure is not maintained in SCOTCH (we discuss this in additional detail in §4.1).

Within these HEALPixels, we select CosmoDC2 galaxies with $r < 28$, which removes the majority of galaxies that were not detected within the DC2 5-year image co-add catalogues. We further refine this sample by removing objects with unreported image properties. This selection yields a sample of ~ 40 million galaxies, which represent a realistic magnitude-limited ($r < 28$) galaxy sample. In Section 5.3, we describe the process of selecting galaxies that match observed properties of transient hosts; this further reduces the sample to ~ 10 million galaxies.

² <https://zenodo.org/record/6601211#.Ypjd6pDMLhM>

³ <https://github.com/spotify/annoy>

⁴ <http://healpix.sourceforge.net>

⁵ <https://github.com/LSSTDESC/gcr-catalogs>

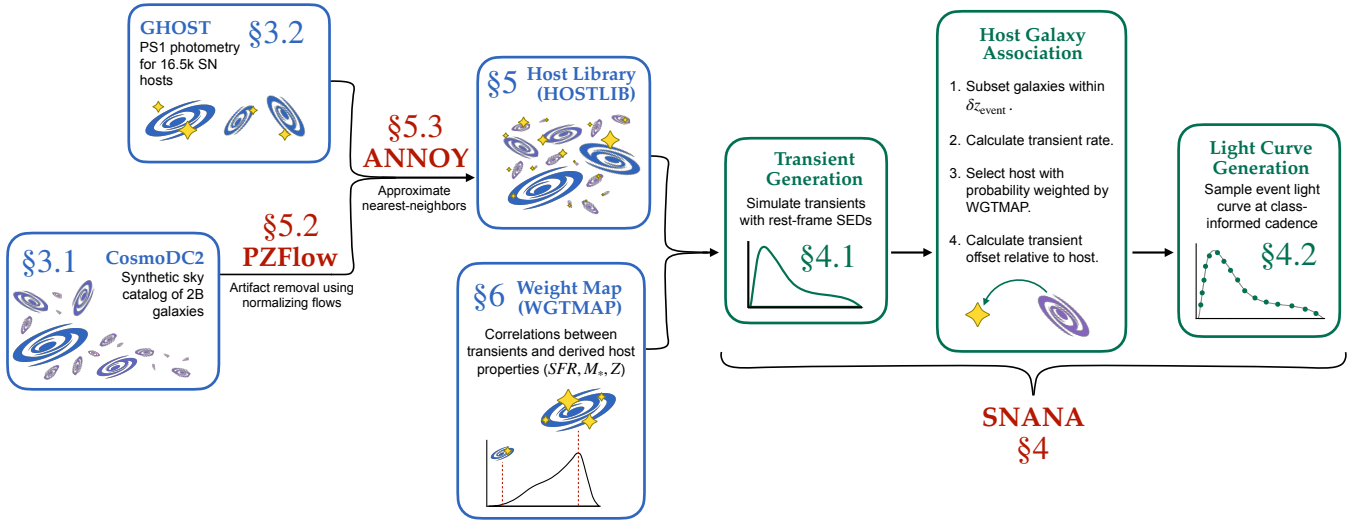


Figure 1. Analysis flowchart with section labels. Intermediate catalogues and data products are given in blue text, major software packages in red text, and methodology in green text.

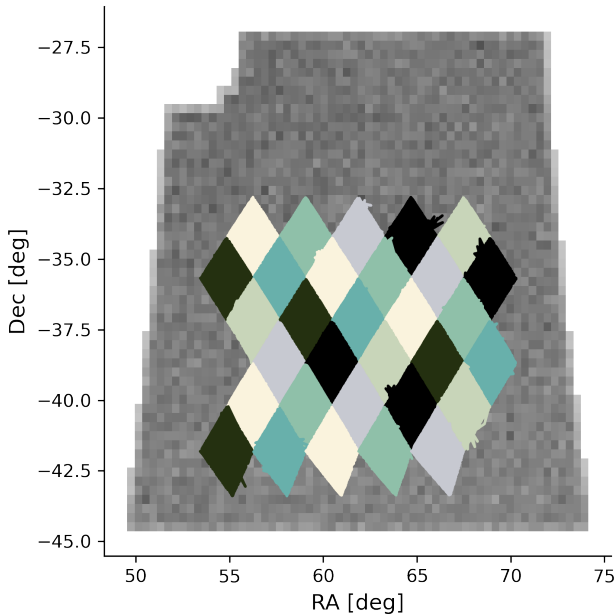


Figure 2. Selected HEALPixels from CosmoDC2 (diamonds) overlaid on the grayscale distribution of object number densities in the DC2 image catalogues. We cross-match CosmoDC2 and the DC2 image catalogues for the image properties of extragalactic objects.

3.2 The GHOST Catalogue of Transient-Host Galaxies

The GHOST catalogue (Gagliano et al. 2021) consists of $\sim 16,500$ archival SNe consolidated from the Transient Name Server (TNS) and the Open SN Catalogue (OSC), as well as the observed properties of their host-galaxies from the first data release of Pan-STARRS (PS1; Chambers et al. 2016). Host galaxies within the catalogue were identified and validated through a combination of the established Directional-Light Radius method (DLR; Gupta et al. 2016) and the Gradient Ascent method (Gagliano et al. 2021). Although

this GHOST sample contains realistic statistical correlations between transients and their host galaxies, it does not contain a representative sample of events anticipated from upcoming surveys. First, the catalogue comprises a small number of low-redshift ($z < 0.2$) explosions. LSST will dramatically enhance our current discovery rate for luminous SNe, motivating the need to scale the sample sizes in the GHOST catalogue for every class. Further, GHOST does not include non-SN transients such as Tidal Disruption Events (TDEs) and Active Galactic Nuclei (AGN), classes whose discovery and characterization are key science drivers for LSST. Finally, because the catalogue contains only the photometric properties of SN host galaxies, it lacks an explicit correlation between a transient and the stellar-mass and star formation rate of its host galaxy.

The CosmoDC2 catalogue provides photometry in LSST ($ugrizY$) and SDSS ($griz$) filters, while GHOST galaxy photometry is provided only in the PS1 ($grizy$) filter system. To accurately match galaxy photometry between these catalogues, we convert the GHOST photometry from the PS1 to the SDSS system. We use the approximate quadratic conversions defined in Tonry et al. (2012) and k -correct the apparent magnitude in each band using the analytic approximations⁶ described in Chilingarian et al. (2010) and Chilingarian & Zolotukhin (2012). This transformation allows us to accurately match GHOST galaxies to those in CosmoDC2. Next, we use the spectroscopic redshift of each galaxy’s associated transient (or the spectroscopic redshift of the host, if the former was unreported on TNS) to calculate the absolute rest-frame brightness of each galaxy in SDSS pass-bands. We use these to compute rest-frame $g-r$, $r-i$, and $i-z$ colours. To ensure that only galaxies with high-SNR photometry are considered, we apply stringent quality cuts to the galaxies in the GHOST sample based on the values of the PS1 primaryDetection and objInfoFlag flags, as well as the InfoFlag1, InfoFlag2, and InfoFlag3 values in each band.⁷ While this may limit our observed sample to only low-redshift events, it ensures that the photometric

⁶ <http://kcor.sai.msu.ru/getthecode/#python>

⁷ A full list of the imposed quality cuts can be found at the github repository for this work.

correlations we encode from this regime are accurate. Our final sample after these cuts consists of 8,800 SN host galaxies.

4 GENERATING TRANSIENTS WITH THE SNANA SIMULATION

4.1 The SNANA Framework for Generating Transients

Our methodology is shaped by the existing framework of the SNANA simulation code (Kessler et al. 2009). Therefore, although the use of SNANA constitutes the final stage of our pipeline as displayed in Fig. 1, we first describe the SNANA simulation and introduce the simulation-specific terminology before detailing our methods for host galaxy association. This simulation reads user-defined transient model SEDs (rest-frame), redshift-dependent rates, and realistic observing conditions, and outputs transient events with realistic light curves and spatial distributions as a function of redshift. The SNANA simulation was used to generate 9 different extragalactic transient classes for PLAsTiCC; Figure 1 from Kessler et al. (2019) shows example output light curves in *ugrizY* bands from each model. In this paper, we distinguish SNe Ib from SNe Ic and SNe II_n from SNe II to simulate 11 classes: AGN, KN, TDE, SLSN-I, SN Ib, SN Ic, SN II, SN II_n, SN Iax, SN Ia-91bg, and SN Ia, with the addition of SN IIb and SN Ic-BL and with some updates to the PLAsTiCC models as described in §4.2. We adopt the default SNANA cosmology, which sets the cosmological parameters to $\Omega_M = 0.315$, $\Omega_\Lambda = 0.685$, $w_0 = -1$, and $H_0 = 70 \text{ km s}^{-1} \text{ Mpc}^{-1}$. The transient models differ in the distributions of emission across bands, the shape of the light curves, and the peak brightness. For example, most of the SN Ib/c model flux is emitted at redder wavelengths; the KN model exhibits a characteristic timescale shorter than most other transients in our sample; and simulated SLSNe-I emit significantly higher flux than the other models.

The SNANA simulation includes the option of associating each simulated transient to a host galaxy from a user-input catalogue (the *host library* or ‘HOSTLIB’) that includes redshift and other galaxy properties (§5). After each transient is simulated, the algorithm selects a HOSTLIB galaxy that lies within δz of the transient. We set δz to correspond approximately to 100 comoving Mpc, which ranges from 0.02 at $z \sim 0$ to 0.1 at $z = 3$ given the 2018 cosmological parameters from the Planck satellite (Planck Collaboration et al. 2020). Host galaxy selection is further influenced by a user-input *weight map* (WGTMAP) that defines the probability of selecting a galaxy as a function of its properties (§6). The WGTMAP framework is flexible, such that the probability can depend on different galaxy properties for different classes—in other words, dimensionality of each WGTMAP is not fixed but rather user-defined.

Following Fig. 1, the simulation begins by generating a transient SED and random redshift (following a rate model). Next, the transient is matched to a host galaxy, and the transient offset from the galaxy center is determined probabilistically from the galaxy’s Sersic profile in CosmoDC2. The host galaxy redshift is updated to match the redshift of the transient and the host apparent magnitudes are updated to reflect the small change in distance (100 comoving Mpc or less). With this framework, one host galaxy from the HOSTLIB can be used multiple times, in which case it is mapped to multiple independent galaxies with slightly different redshifts and apparent magnitudes in the final catalogue. The transient SED is modified for cosmic expansion and redshift, and the top-of-the-galaxy SED (including host galaxy extinction but no Galactic extinction or atmospheric effects) is converted to an apparent magnitude in the LSST photometric system (*ugrizY*).

HOSTLIB	WGTMAP	Class	Cadence (Days)
SN Ia Hosts	P_{Ia}	SN Ia	2.0
SN II Hosts	P_{II}	SN II/II _n /IIP/IIL	2.0
H-Poor SN Hosts	P_{Ibc}	SN Ib/Ic	2.0
	$R_{\text{Ic-BL}}$	SN Ic-BL	2.0
	P_{SLSNI}	SLSN-I	2.0
	P_{II}	SN IIb	2.0
Rand. DC2 Subset	P_{AGN}	AGN	0.1, 2.0
	R_{KN}	KN	0.1–2.0
	P_{TDE}	TDE	0.1–2.0

Table 1. Summary of the HOSTLIB, WGTMAP, and cadence used for each transient class in our simulation. The first three HOSTLIBs contain CosmoDC2 galaxies that extrapolate distributions of observed hosts in GHOST; the fourth is a representative sample from CosmoDC2. P_{class} refers to the probability of each transient class occurring given the properties of a galaxy; these functions are defined in §6 and implemented via the WGTMAPS. The cadence refers to the time interval between light curve samples in the simulation.

We sample most of our simulated light curves from 100 days preceding peak light to 100 days after peak. Due to the rapid rise and decline of KN photometry, we sample the light curve for only 10 days pre-peak and 60 days after-peak. For each transient class, we implement one of three cadence strategies. For SNe Ia, CCSNe (II, II_n, IIP, and IIL), and H-poor SNe (Ib/c, Ic-BL, IIb, SLSN-I), we adopt a relatively coarse sampling of $\delta t = 2.0$ days (so that each light curve has 100 observations each in *ugrizY*). Because of the rarity of high-cadence KN and TDE observations, we aim to preserve as much physical information about these light curves as possible while keeping file sizes manageable. For these events, we adopt a logarithmic sampling scheme with $\delta t = 0.1$ d at peak and increasing toward $\delta t = 2.0$ d in either temporal direction. Because the rise of many transient light curves occurs on significantly shorter timescales than a decline powered by emission from radioactive decay, our cadence increases more slowly from peak light to late times than from peak light to pre-explosion epochs (Fig. 3). This sampling scheme generates ~ 260 observations per pass-band. The rapidly-evolving stochasticity of AGN light curves cannot be accurately characterized by either of these cadences. For the AGN in our catalogue, we provide light curves at cadences of both $\delta t = 0.1$ d (250 events) and $\delta t = 2.0$ d (2,250 events). The choice in light curve can be made by the user, depending on their science goals. We show the cumulative number of observations for our three light curve sampling cadences, along with sample light curves, in Fig. 3.

We provide a summary of the classes of transients generated in this work, the HOSTLIBs and WGTMAPS used to associate them with hosts, and the sampling method for each class, in Table 1.

Because we aim to construct a catalogue that can be used for simulating transient discovery across multiple upcoming surveys, we do not realistically place simulated transients across the sky. Further, we do not preserve the original CosmoDC2 galaxy coordinates. Including the full spatial information of CosmoDC2 galaxies would require using each HOSTLIB galaxy no more than once, which in turn requires very large HOSTLIBs given the desired number of transients (5M) that we aim to simulate. While this is not impossible, it requires an alternative setup and additional computational time. We leave an accurate embedding of transients within the cosmic web to future work.

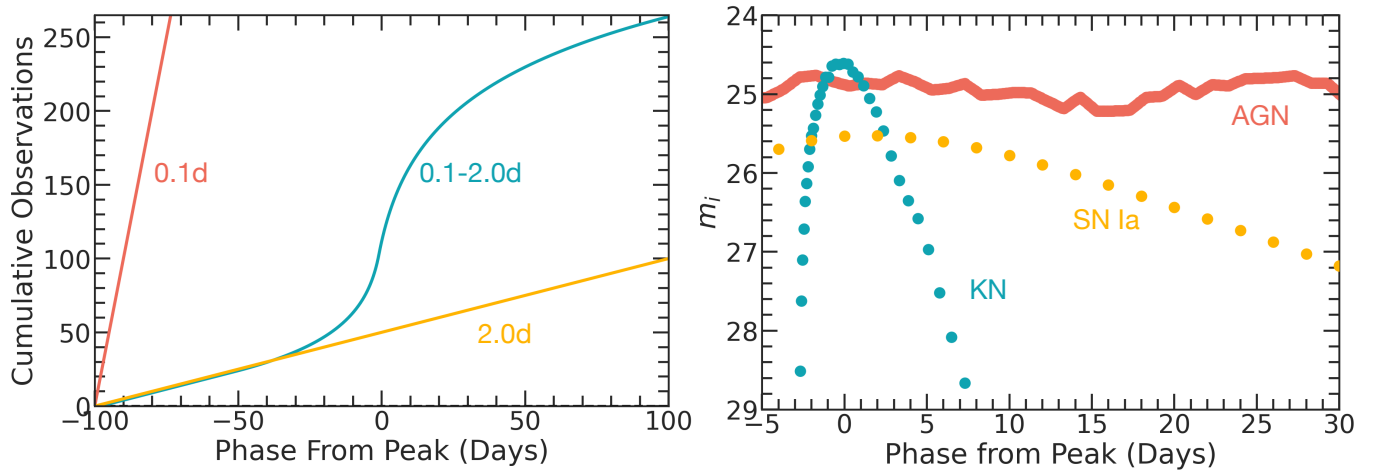


Figure 3. Left: Number of cumulative observations for the variable-cadence ($0.1d \leq \delta t \leq 2.0d$) light curve sampling method for KNe (turquoise), shown alongside the $\delta t = 0.1d$ (red) and the $\delta t = 2.0d$ (yellow) cadences. The function describing the variable-cadence sampling rate is asymmetric in time to mimic the rapid rise and slow decay of transient phenomena. Right: Sample light curves for events using these cadences. Colours indicate the sampling method used.

4.2 Transient Models

We simulate each transient class with a similar setup as that of the PLAsTiCC challenge (see [Kessler et al. 2019](#), hereafter K19, and references therein). Unless otherwise noted, the event rate of each class follows the same redshift dependency as in PLAsTiCC. As detailed in K19, the redshift-dependent rates have been measured from existing observations, and thus become increasingly uncertain with redshift. We extrapolate the rates to $z = 3$ for SCOTCH, but caution that the rate functions are unlikely to be trustworthy at high redshifts. We are unable to simulate realistic *volumetric* rates with the framework described, as our ideal ‘observing’ conditions and wide redshift range would generate a prohibitively large catalogue. Instead, we choose to simulate 5 million events and divide the sample by class based on anticipated interest to users. The sky density of events at any given redshift, and the relative rates of different classes, is therefore inaccurate. Table 2 displays the number of light curves and model used per class. The true expected number of objects per year for each class and model, given the volumetric rates from K19, is reported in Appendix B3 for interested catalog users. We simulate normal and peculiar SNe Ia using the same models used in K19. Additionally, the core-collapse SN models suffixed with MMF, Templates, and MOSFIT in Table 2 are identical to those detailed in K19. However, several features of our simulation are different than PLAsTiCC. We do not include the parametric SNIbc MOSFIT model, which was part of PLAsTiCC, because its parameters were drawn from unrealistic flat distributions and the models produce unphysical light curves. We also add the recent core-collapse spectrophotometric templates from [Vincenzi et al. \(2019\)](#), which are suffixed by HostXT_V19 in Table 2. The V19 models add realistic diversity to our core-collapse sample. The V19 models include templates for SNe IIB and SNe Ic-BL, which are both new since PLAsTiCC. SN Ic-BL are energetic Ic events observed with broad lines in their spectra, indicating enhanced absorption velocities of $\sim 15,000\text{--}30,000 \text{ km s}^{-1}$ ([Modjaz et al. 2016](#)). Thus, the Ic-BL templates are distinguishable from the typical Ic model primarily through spectroscopy. As we only simulate photometric light curves for SCOTCH, the only relevant difference from SNe Ic is that SN Ic-BL light curves are brighter.

The SLSN I, TDE, and AGN models are similar to those in K19,

the only difference being that we impose an upper redshift limit of $z = 3$ to match the limit of CosmoDC2 galaxies within the HOSTLIBs.

PLAsTiCC included a set of kilonova SED models from [Kasen et al. \(2017\)](#). In this work, we incorporate the Kasen model as well as an SED model by [Bulla \(2019\)](#). Both approaches parametrize the rapidly decompressing ejecta from the merger of two neutron stars that are heated by radioactivity from r-process nucleosynthesis. The [Bulla \(2019\)](#) model⁸ is parameterized by the mass of the ejecta, the half-opening angle of its lanthanide-rich component, and the angle between the line of sight and the plane of merger. The [Kasen et al. \(2017\)](#) models consider the SED parameterized by the ejecta mass, the lanthanide fraction, and the ejecta velocity, without an observing angle dependence. In general, larger values of the ejecta mass lead to brighter events, while increasing the lanthanide fraction leads to redder, longer-lived kilonovae. Both models are grid-based, i.e., an SED given on a grid of discrete model parameters. Recently, [Chatterjee et al. \(2021\)](#) incorporated the Bulla model into SNANA, and used both these kilonova models to create a classifier to filter kilonovae from other astrophysical transients using photometric and contextual information available from gravitational wave data products. The SED data for both the models are publicly available as part of the SNANA package.⁹

We present the distribution of lightcurves for a representative sample of each simulated transient class in Fig. 4. We further present the redshift distribution of simulated AGN, SNe Ia, SNe II, and SLSNe-I in Fig. 5.

5 HOST LIBRARY CREATION (HOSTLIB)

5.1 Overview

Our first step to realistically associate transients with hosts is to create HOSTLIBs from CosmoDC2 galaxies. In previous work, including [Vincenzi et al. \(2021\)](#), HOSTLIBs were constructed of representative field galaxies and correlations with transient class were implemented

⁸ We consider the two-component model here; “BULLA-BNS-M2-2COMP” in SNANA package data.

⁹ <https://doi.org/10.5281/zenodo.4728252>

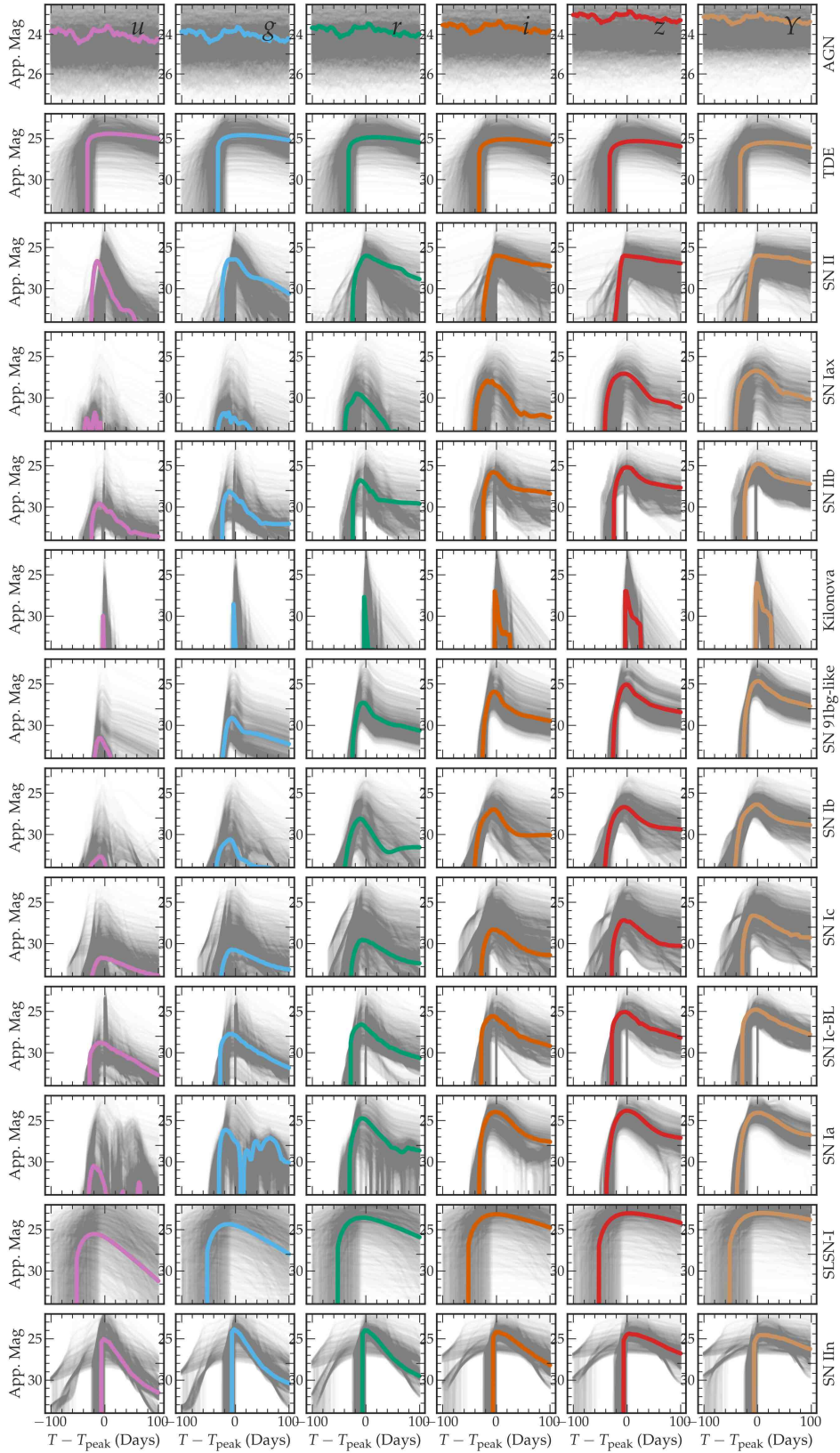


Figure 4. Light curves for the transient classes simulated in this work. Gray curves show a representative sample of events, and coloured curves show one example event for each class. Due to the rapid rise of the kilonova model, few KN light curves feature emission at epochs prior to peak light.

Class	Model name	N
Ia (2.2M total)	SALT2-Ia	2M
	Iax	100,000
	91bg-like	100,000
H-Rich Core-Collapse (1,999,000 total)		
SN II (1.9M total)	SNII-Templates	633,000
	SNII-NMF	633,000
	SNII+HostXT_V19	633,000
SN IIn (100,000 total)	SNIIIn-MOSFiT	50,000
	SNIIIn+HostXT_V19	50,000
Stripped Envelope / H-Poor Core-Collapse (500,000 total)		
Ib (100,000 total)	SNIb-Templates	50,000
	SNIb+HostXT_V19	50,000
Ic (100,000 total)	SNIc-Templates	50,000
	SNIc+HostXT_V19	50,000
IcBL	SNIcBL+HostXT_V19	100,000
Iib	SNIIb+HostXT_V19	100,000
SLSN-I	SLSN-I-MOSFiT	100,000
Non-SN Transients (301,000 total)		
KN (100,000 total)	Kasen 2017	50,000
	Bulla 2019	50,000
TDE	TDE_MOSFiT	101,000
AGN	AGN-LSST	100,000

Table 2. Simulated transients in the SCOTCH catalogue organized by class and model name. N , the number of transients simulated per class, sums to 5 million.

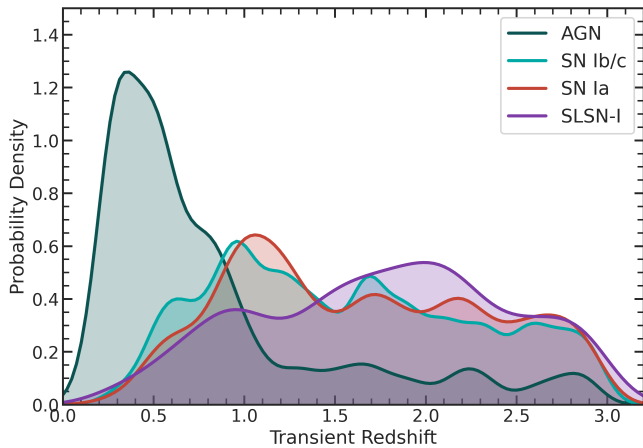


Figure 5. Kernel density estimates of the redshifts for a representative sample of four classes in SCOTCH. Distributions reflect the class-specific event rates used in the simulation.

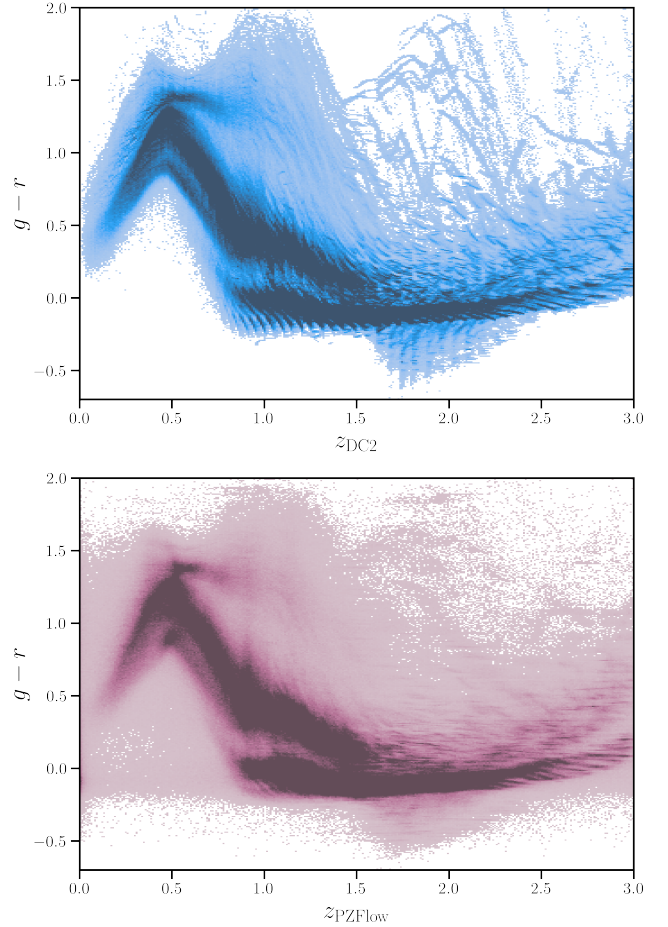


Figure 6. **Top:** $g-r$ colour versus redshift for galaxies within the CosmoDC2 synthetic sky catalogue (Korytov et al. 2019). Discrete tracks visible in this space are an artifact of the limited number of SED models used to generate the derived properties of these galaxies. **Bottom:** The same $g-r$ values plotted against redshifts drawn from a probability density function estimated using a normalizing flow (Crenshaw et al. 2021). There is a one-to-one mapping between the galaxies in the top and bottom image; each galaxy’s redshift is slightly shifted, which smears out many of the non-physical tracks.

solely via the WGTMAP schema. However, WGTMAPs that depend on more than a few host properties N are prohibitively memory-intensive and computationally slow, as the SNANA code requires weights to be defined over an evenly-spaced grid across the full N -dimensional parameter space. To incorporate additional galaxy properties in our transient-host association, we generate *tailored* HOSTLIBs for different transient categories containing correlations in host galaxy colour and magnitude.

5.2 Accounting for CosmoDC2 Artifacts with PZFlow

The distribution of CosmoDC2 galaxies in colour-redshift space contains non-physical structure that worsens at higher redshifts. The problem is caused by a mismatch between the colour ranges in different components of the hybrid catalogue production pipeline for CosmoDC2 (Korytov et al. 2019), and manifests as discrete ‘tracks’ in colour-redshift space across the full redshift range (upper panel of Fig. 6). These artifacts limit our ability to test upcoming machine-learning based photometric redshift estimators. Along each track, the dispersion about the colour-redshift relation is unrealistically

low. Photometric redshift and classification algorithms trained using these data are likely to achieve unrealistically accurate results. As photo- z estimation is an important component of upcoming large-sky transient and galaxy surveys, we mitigate this effect by smearing the streaky colour-redshift relationship for selected CosmoDC2 galaxies.

We use the code PZFlow¹⁰ (Crenshaw et al. 2021) realistically shift galaxy redshifts and smear the colour-redshift tracks. PZFlow uses normalizing flows (Jimenez Rezend e & Mohamed 2015) to efficiently model a multi-dimensional probability density function (PDF). The normalizing flow learns a bijection, a function which maps the PDF to a tractable latent distribution (such as a uniform distribution) in which we can easily sample points and calculate densities. We use a normalizing flow to model the conditional PDF $p(z|\mathbf{m}, M_*, \text{SFR})$, where \mathbf{m} is a vector of LSST $ugrizY$ apparent magnitudes. The latent distribution for the flow is a uniform distribution over the range $[-5, 5]$. The bijection consists of two layers: the first layer shifts the redshift range $[0, 3]$ into the range of the latent uniform distribution, $[-5, 5]$; the second layer is a Rational-Quadratic Neural Spline Coupling (RQ-NSC; Durkan et al. 2019), which transforms the redshift distribution into a uniform distribution. The RQ-NSC performs this transformation using splines parameterized by a set of knots. The number of spline knots, K , can be chosen to increase or decrease the resolution of information captured by the flow. We choose a low value of $K = 2$ so that the flow does not learn the discrete tracks in the CosmoDC2 colour-redshift space, and instead smooths over them.

We train the normalizing flow on the CosmoDC2 galaxies for 30 epochs using maximum likelihood estimation. Then, for each galaxy, we sample a new redshift z_{PZFlow} from the normalizing flow. These new redshifts are consistent with the galaxies' photometry, stellar masses, and star formation rates, but are slightly perturbed from their original values (see left and middle panels of Fig. 7). For 92% of the galaxies, the change in redshift is $\delta z < 0.1$. While 8% of redshifts have more substantial perturbations, we stress that each perturbed redshift is consistent with that galaxy's photometry, stellar mass, and star formation rate. It should not be surprising that, for some galaxies, a substantially different redshift remains consistent with its other properties (Salvato et al. 2019).

We adjust each galaxy's absolute magnitude to be consistent with its apparent magnitude given its new luminosity distance. The right panel of Fig. 7 shows the size of these adjustments. For 93% of galaxies, the absolute magnitude change is $\delta M < 0.2$. We expect the small magnitude perturbations to lie within the realistic scatter of galaxy properties.

We have perturbed the galaxy redshifts with the goal of removing the discrete tracks in colour-redshift space that would lead to overly-optimistic photo- z estimates. We present the original and re-sampled redshift distributions in the upper and lower panels of Fig. 6, respectively, in which only a fraction of the tracks remain (and these are primarily at very high redshift).

After applying PZFlow, we perform an additional cut to clean the CosmoDC2 rest-frame colour distribution. We limit our sample to galaxies with $-0.18 < i - z < 0.5$, which maintains the vast majority of the CosmoDC2 colour distribution but removes two unrealistic clumps that were apparent on the red and blue extremes.

5.3 Selecting a CosmoDC2 subsample

Ideally, we would sample directly from the CosmoDC2 galaxies, with our selection informed by real data, to populate a catalogue of synthetic host galaxies for each transient class. Although the GHOST dataset includes many SN classes, for most classes (e.g., SNe IIn, Ic-BL, and IIB) the sample size is too small to contain representative information. To combat this issue, before matching we group the hosts of archival GHOST SNe into three larger categories:

- (i) 6,284 hosts of Type Ia SNe.
- (ii) 1,973 hosts of core-collapse SNe with hydrogen lines in their spectra, including those classified as Type II, IIn, and IIP.
- (iii) 443 hosts of hydrogen-poor SNe, including stripped-envelope core-collapse SNe and hydrogen-poor superluminous SNe (SLSNe-I).

For each group, we select a many-times larger sample of synthetic CosmoDC2 galaxies that approximates the distribution in GHOST galaxy properties while extending to higher redshifts. We construct a HOSTLIB for each of these 3 broad categories.

With insufficient high- z data to model any cosmic evolution of transient-host correlations, a reasonable approach to high-redshift HOSTLIB sampling is to find high- z CosmoDC2 galaxies with similar intrinsic properties as low- z galaxies; e.g., rest-frame absolute magnitudes, rest-frame colours, and morphology. This approach ignores the possible evolution of transient-host correlations over cosmic time.

We employ a nearest-neighbour (NN) technique, illustrated in Fig. 8, to achieve this matching. NN algorithms deteriorate in high-dimensional space due to decreased data density, so we select a small number of galaxy properties that are most correlated with transient properties. We train our NN matching on absolute rest-frame r - and i -band magnitudes, rest-frame $g-r$ and $i-z$ colours, and the PZFlow-shifted redshifts. This combination of properties incorporates information from all $griz$ bands (u and y being unavailable after converting GHOST data to SDSS filters) without redundancy. Although a similar matching could be achieved by simply using the $griz$ magnitudes and allowing colour to be implicitly included, doing so would down-weight the importance of color. We choose to explicitly make two of the four dimensions colors, with an even weighting as the magnitudes, because both are highly correlated with galaxies' likelihoods to host transients. We manually down-weight redshift with respect to the colours and magnitudes to allow for neighbour matching across a wide range of redshifts. We considered also matching on morphological information such as galaxy radius and ellipticity, but found the difference between observational and simulated estimates to be prohibitive given the necessary corrections to systematics in the GHOST data (e.g., deconvolving the PSF from ellipticity and radius measurements) and the strong redshift-dependent observational bias towards intrinsically large galaxies in targeted surveys.

Although exact NN algorithms (e.g., scikit-learn's KNeighbours) are sufficient for samples of $N \sim 10^5$, they become increasingly slow when scaling up to $\sim 10^7$ galaxies. Instead, we make use of a rapid approximate NN method called ANNOY, which leverages Locality-Sensitive Hashing (LSH; Datar et al. 2004), to rapidly cross-match datasets in parallel. We provide additional information on our use of this method in Appendix A. We select k neighbours in CosmoDC2 with low Euclidean distance (d_{ANNOY}) to each GHOST galaxy. Rather than impose a limit on d_{ANNOY} , we set k to a value that produces several million matched CosmoDC2 galaxies. We then remove synthetic galaxies that were matched to multiple GHOST galaxies, creating HOSTLIBs with ~ 1 million ob-

¹⁰ <https://github.com/jfcrenshaw/pzflow>

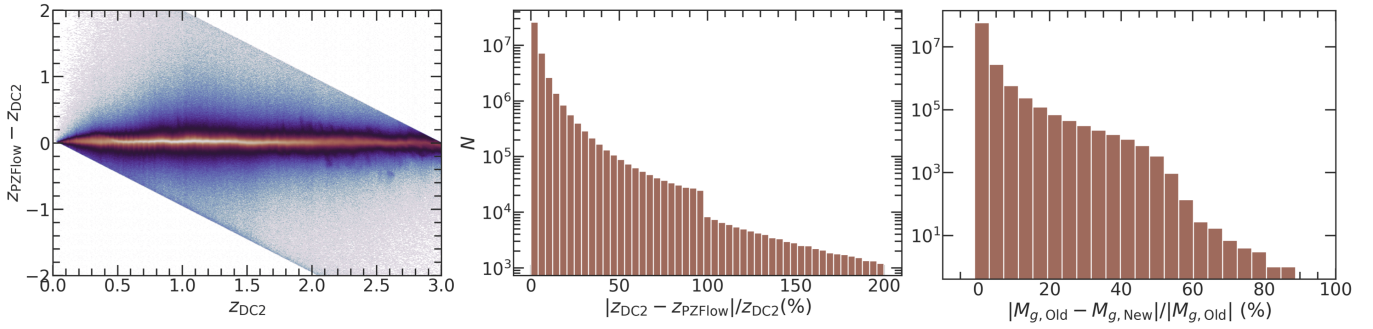


Figure 7. **Left:** Difference between PZFlow-sampled redshift and original CosmoDC2 redshift as a function of CosmoDC2 redshift for each galaxy in the sample. Shifts are minimal, and the discrete paths at top left and bottom right reflect the bounds of $[0, 3]$ imposed in generating PZFlow samples. **Middle:** Histogram of fractional differences in galaxy redshift before and after the PZFlow-oversampling stage. **Right:** Histogram of fractional differences in absolute magnitude propagated from the PZFlow-shifted redshifts.

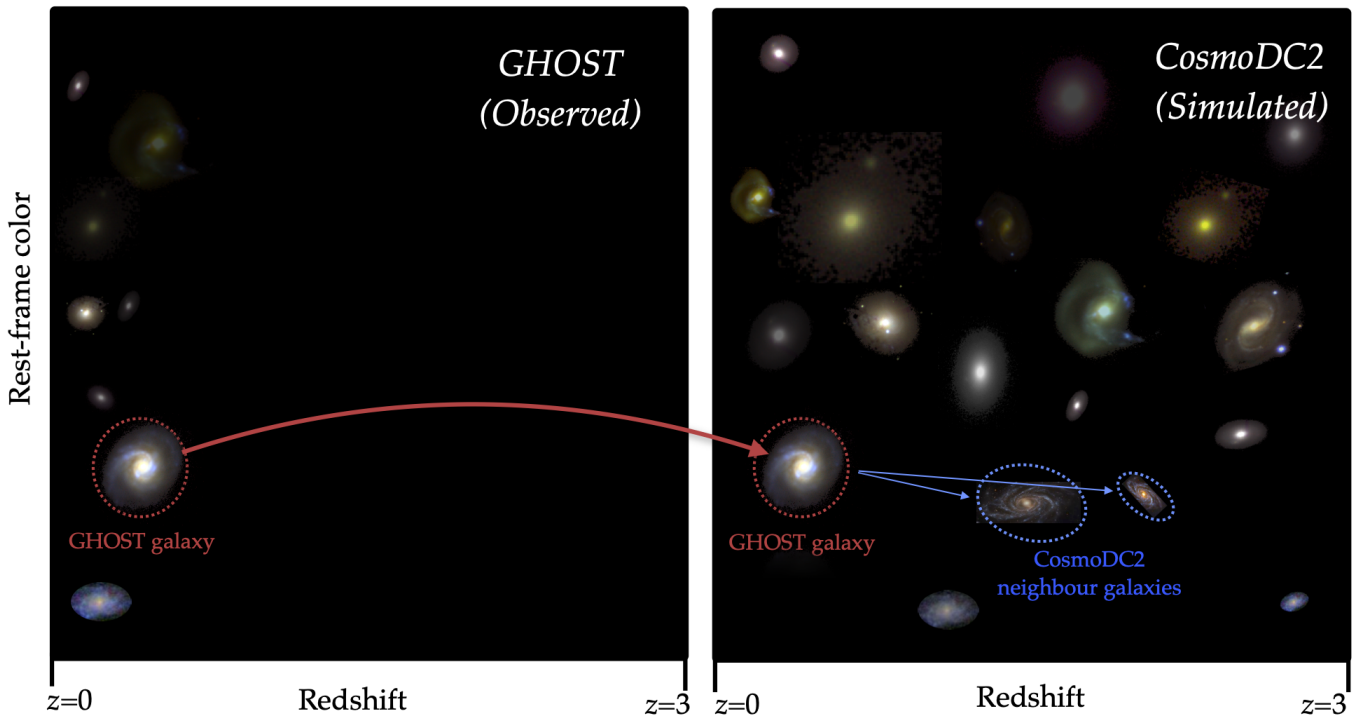


Figure 8. Illustration of CosmoDC2 sampling for HOSTLIB generation. **Left:** We identify GHOST galaxies which hosted transients belonging to a particular category (the three categories are defined in the text). The GHOST sample is observationally biased toward low-redshift, but we assume the rest-frame properties (like color, shown on the y axis) are representative of the true full sample of hosts. **Right:** For every GHOST galaxy, we select k synthetic galaxies from CosmoDC2 nearby in rest-frame color, brightness, and redshift (with small d_{ANNOY} values; see appendix for details) but extending to $z = 3$. For simplicity, the diagram shows $k = 2$ and a 2-dimensional parameter space; in practice, however, $k = 800 - 18,000$ and 5 parameters are used for matching.

jects each. This requires k to range from 800-18,000 across the three host categories.

Using this pipeline, we generate HOSTLIBs of CosmoDC2 galaxies matching the host-galaxy distributions in GHOST for the three groups of transient classes described above. We show the distribution of observed GHOST galaxies, a random subset of CosmoDC2 galaxies, and the final matched sample for the Hydrogen-poor host group in Fig 9. In addition to the three HOSTLIBs described above, we create a HOSTLIB consisting of galaxies randomly sampled from CosmoDC2 for transient classes not in the GHOST catalogue. The host correlations for events using this unmatched HOSTLIB originate entirely from the transient-specific WGTMAP.

The CosmoDC2 simulation contains many ultra-faint galaxies that were injected into the simulation to account for its finite mass resolution (Korytov et al. 2019). These galaxies were not assigned properties as rigorously as the normal galaxies in the simulation; as a result, we exclude them from our HOSTLIBs. Our initial $r < 28$ cut on CosmoDC2, as well as the matching to GHOST galaxies (which are generally bright), remove many of these galaxies from our sample. We identify any remaining ultra-faint galaxies by their negative `halo_id` after HOSTLIB creation and cut them from the samples.

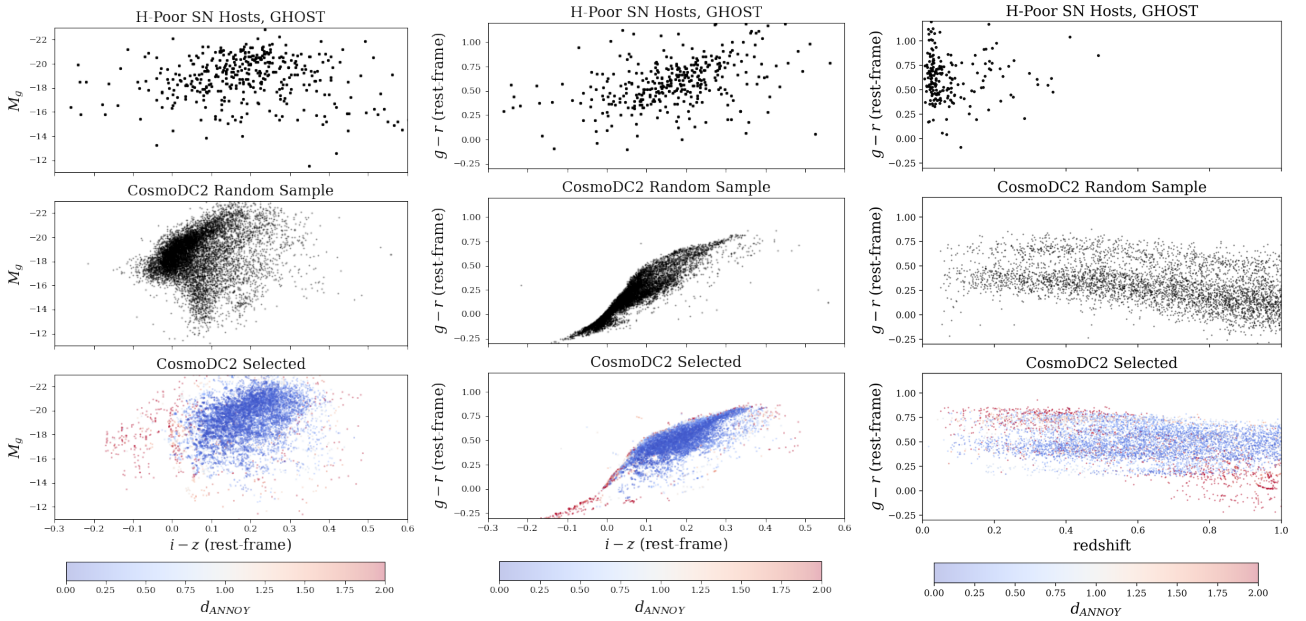


Figure 9. A representation of how the GHOST-CosmoDC2 matching process produces a larger sample of GHOST-like galaxies from CosmoDC2. Each set of three panels (stacked vertically) show the same steps of the process which creates the H-poor host library. The left three plots show a magnitude-colour distribution, the middle show colour-colour space, while the right show colour vs. redshift. **Top:** the GHOST H-poor event host galaxies. **Center:** a random subset of CosmoDC2 galaxies. **Bottom:** nearest-neighbour galaxies selected from CosmoDC2 to match each GHOST galaxy in a multidimensional parameter space. The colour bar, applying only to the bottom three plots, signifies the nearest-neighbour Euclidean distance and is truncated at 2 for visual purposes. Red points are CosmoDC2 galaxies that are far from their nearest GHOST neighbour. From the left and center plots, it is apparent that the limited colour ranges in CosmoDC2 also limit the effectiveness of matching, as some GHOST galaxies lie beyond the available DC2 colour extent. The right plots demonstrates how down-weighting redshift as a matched property allows us to select CosmoDC2 galaxies across a wide range (extending to $z = 3$, but only shown up to $z = 1$).

6 TRANSIENT-HOST GALAXY CORRELATIONS (WGTMAP)

The GHOST database contains only basic photometric properties for SN host galaxies. Additional properties like masses and star formation rates, which can be estimated from galaxy imaging and/or spectra, are not reported in GHOST due to the lack of availability. Thus, the HOSTLIBs of CosmoDC2 galaxies matched to GHOST are realistically distributed in colour and brightness, but only contain an implicit dependence on derived properties that cannot be directly validated. There is motivation to fold in explicit dependence on mass and star formation rate: many studies have empirically verified this dependence for multiple transient classes (using smaller samples than GHOST) and found statistically significant differences between classes. We construct a series of WGTMAPs that explicitly encode the dependence of host-transient association on derived properties for each class. These WGTMAPs enable us to fine-tune the host populations of the three matched HOSTLIBs and add in class-specific correlations for events whose hosts will be drawn from the unmatched, randomly-sampled HOSTLIB.

Each WGTMAP consists of a multidimensional grid of host properties, where values in the grid correspond to the probability of a host with those properties being selected to match a given transient event in SNANA. The weightmap values can be scaled arbitrarily, so long as the *relative* weights between galaxies of different properties are correct. When the SNANA simulation generates a transient at z , its host is selected from the sample of HOSTLIB galaxies within Δz . For each possible galaxy with given properties, SNANA assigns the corresponding weight from the WGTMAP. The simulation creates a cumulative distribution function (CDF) for all galaxies, where the horizontal axis orders the galaxies arbitrarily, and the function is

augmented by each galaxy’s weight. The CDF is normalized to have a maximum value of one. The simulation selects a random number for the CDF vertical axis, and picks the corresponding galaxy along the horizontal axis, such that highly weighted galaxies have a higher CDF slope and are therefore more likely to be selected. Because the normalization is computed internally within SNANA, only the *proportionality* linking the probability P to the host galaxy parameters must be defined for the WGTMAPs.

The following subsections review the probabilities used to generate the WGTMAPs of each class. We caution that for several classes (TDEs, KNe, SNe Ic-BL, and SLSNe-I), the data statistics remain limited and thus the resulting simulations may not capture the full diversity of host galaxies. Fig. 10 provides some intuition for the probability equations that follow by showing the resulting SFR-mass distribution of hosts selected by SNANA from these equations for six classes.

6.1 SNe Ia

SNe Ia explosions are thought to occur when a white dwarf accretes material from a companion star (which may also be degenerate) in a binary system, approaching the Chandrasekhar mass and igniting a runaway chain reaction of carbon fusion. SNe Ia occur more frequently in high-mass and highly star-forming galaxies (Sullivan et al. 2006; Smith et al. 2012; Wiseman et al. 2021). Their light curves are parameterized in the SNANA simulation using the Spectral Adaptive Lightcurve Template (SALT2/SALT3) frameworks (Guy et al. 2007a; Kenworthy et al. 2021).

The probability of SNe Ia as a function of galaxy properties can be written as a multiple of two components:

$$P_{\text{Ia}}(M_*, \text{SFR}, x_1) = P_{\text{Ia}}^{\text{KDE}}(M_*, \text{SFR}) \times P_{\text{Ia}}^*(x_1, M_*) \quad (1)$$

where M_* is the host galaxy stellar mass, SFR is its star formation rate, and x_1 is the SALT2 stretch parameter of the SN light curve (Guy et al. 2007b).

The first component of the probability, $P_{\text{Ia}}^{\text{KDE}}$, encodes a dependence on galaxy stellar mass and star formation rate. It has been constructed to replicate the distribution of 200 SN Ia host galaxies from the Dark Energy Survey Supernovae Program (Smith et al. 2020). Using the `statsmodel` Python package, we perform kernel density estimation on the DES $\log(M_*)$ and $\log(\text{SFR})$ values to estimate a smooth probability density function in $\log(M_*)$ vs. $\log(\text{SFR})$ space. We use a Gaussian kernel for both parameters and determine the best-fit bandwidths from the KDE fit, finding 0.49 and 0.47 for $\log(M_*)$ and $\log(\text{SFR})$, respectively. Because $P_{\text{Ia}}^{\text{KDE}}$ is a non-parametric estimate for the probability density of observed events, it has no closed form.

The second component represents the anti-correlation between M_* and x_1 as shown in Fig. 4 of Smith et al. (2020). Based on the fact that few events have been observed with $M_* < 10^{10}$ and negative x_1 , we implement the following model from Vincenzi et al. (2021):

$$P_{\text{Ia}}^*(x_1, M_*) \propto \begin{cases} e^{-x_1^2}, & \text{for } x_1 < 0 \text{ and } M_* < 10^{10} \\ 1, & \text{for } x_1 > 0 \text{ and } M_* < 10^{10} \\ 1, & \text{for } \forall x_1 \text{ and } M_* > 10^{10} \end{cases} \quad (2)$$

6.2 Peculiar SNe Ia

In addition to ‘normal’ SNe Ia, our simulated sample includes two classes of peculiar transients: SN2002cx-like SNe (SNe Iax; Foley et al. 2013), which are underluminous and red at peak light relative to their Branch-normal counterparts; and 1991bg-like SNe Ia, which are more rapidly evolving (Filippenko et al. 1992). Although observed samples are small, there are indications that SNe Iax occur almost exclusively in late-type, star forming galaxies (Jha 2017; Takaro et al. 2020) and SNe 91bg preferentially occur in early-type, passive galaxies (van den Bergh et al. 2005; Hakobyan et al. 2020). Accordingly, Vincenzi et al. (2021) set the SN Iax probability to the SN Ia probability in active hosts and 0 in passive hosts; conversely, they define the SN 91bg-like probability as equal to the SN Ia probability in passive hosts and 0 in active hosts. We adopt a similar approach, assuming that the peculiar SNe Ia originate from similar progenitors as normal SNe Ia but that their hosts represent opposite ends of a continuum in galaxy age and morphology. However, we exponentially taper the probability of SNe Iax in passive galaxies and 91bg-like events in star-forming galaxies. This is done in order to avoid encoding an unrealistically discrete boundary in our catalogue, and to account for the possibility that a sub-population of these events does occur in hosts distinct from those previously discovered.

As in Sullivan et al. (2006) and Vincenzi et al. (2021), we define a threshold between active and passive galaxies at specific star formation rate (sSFR) values of $\log_{10}(\text{sSFR}/\text{Gyr}^{-1}) = -11.5$; active galaxies lie above this threshold and passive galaxies lie below it. For SNe Iax, our combined probability function adopts the normal SN Ia probability (without x_1 dependence) for active galaxies and tapers the probability below the passive/active threshold as follows:

$$P_{\text{Iax}}(M_*, \text{SFR}) \propto \begin{cases} P_{\text{Ia}}(M_*, \text{SFR}), & \text{for } x_s \geq -11.5 \\ P_{\text{Ia}}(M_*, \text{SFR}) \times e^{(x_s+11.5)}, & \text{otherwise,} \end{cases} \quad (3)$$

where $x_s = \log_{10}(\text{sSFR}/\text{Gyr}^{-1})$. The SN 91bg-like probability does the opposite, tapering the probability in a symmetric manner above

the passive/active threshold:

$$P_{91\text{bg}}(M_*, \text{SFR}) \propto \begin{cases} P_{\text{Ia}}(M_*, \text{SFR}), & \text{for } x_s < -11.5 \\ P_{\text{Ia}}(M_*, \text{SFR}) \times e^{-(x_s+11.5)}, & \text{otherwise.} \end{cases} \quad (4)$$

Because P_{Ia} is *not* symmetric about x_s (it increases with galaxy mass and star formation), we note that this formalism results in a higher probability for 91bg-like events to occur in star-forming host galaxies than SNe Iax to occur in passive host galaxies. The SCOTCH contains $\sim 0.1\%$ of SNe Iax in passive hosts and $>25\%$ of SNe 91bg-like in active hosts. This implementation is motivated by previous work (e.g., Hakobyan et al. 2020) showing a larger tail of 91bg-like hosts toward spiral-type morphologies than toward elliptical galaxies for SNe Iax.

6.3 Types II, Ib, and Ic Supernovae (SNe II, SNe Ib/c)

Type II, Type Ib, and Type Ic are three sub-classes of core-collapse SNe. Type II events are characterized by strong Hydrogen emission lines, indicating that an outer Hydrogen shell was present in the progenitor star. Types Ib and Ic lack Hydrogen features, indicating that their outer shell was stripped from the progenitor star prior to explosion. Type Ic also lacks Helium features, indicating that the Helium envelope was also lost. Although SNe IIb are typically grouped with these ‘stripped-envelope’ events, they exhibit weak hydrogen features at early times. As the explosion progresses, the hydrogen emission quickly fades and the light curves begin to resemble those of SNe Ib. Because of their short-lived progenitor systems (typically <50 Myr), core-collapse explosions are predominantly observed in galaxies that are actively forming massive stars. The probability of these events occurring in passive galaxies, in contrast, is suppressed. Active and passive galaxies can be distinguished by their sSFR, defined as the star formation rate of the galaxy per unit of stellar mass.

The probability of these classes of core-collapse supernovae are set to (Vincenzi et al. 2021):

$$P_{\text{II}}(M_*, \text{SFR}) \propto \begin{cases} (M_*/M_{\odot})^{0.16}, & \text{for } x_s \geq -11.5 \\ 0, & \text{otherwise} \end{cases} \quad (5)$$

$$P_{\text{Ib/c}}(M_*, \text{SFR}) \propto \begin{cases} (M_*/M_{\odot})^{0.36}, & \text{for } x_s \geq -11.5 \\ 0, & \text{otherwise} \end{cases} \quad (6)$$

Additionally, we distinguish the hosts of SNe Ic-BL events from the lower-energy class of SNe Ic explosions through the properties of their host galaxies. To do so, we embed a further correlation with host galaxy metallicity. Additional details concerning this correlation are described in Sec. 6.4.

6.4 Type Ic-BL Supernovae (SNe Ic-BL)

It is hypothesized that long-duration gamma ray bursts (IGRBs, lasting longer than ~ 2 seconds) are produced by relativistic jets originating in an SN explosion and interacting with surrounding circumstellar material (Roy 2021). Broad-Lined SNe Ic (SNe Ic-BL) are the only SNe that have been associated with IGRBs, and these explosions have been found to occur in galaxies of lower average metallicity than the less-energetic SNe Ic (Modjaz et al. 2020). A thorough understanding of the host-galaxy correlations of SNe Ic-BL could permit a reconstruction of the physical conditions that give rise to relativistic jets in SNe. To simulate a distinction between SNe Ic and SNe Ic-BL hosts, the WGTMAP probabilities for both SNe Ic and SNe Ic-BL are

constructed as the multiple of two terms. The first term embeds the preference for core-collapse events to occur in active galaxies, which is parameterized by equation 6. For the second term, we consider the metallicity and model the distribution of SN Ic and SN Ic-BL host galaxy metallicities as a set of logistic distributions:

$$P_{\text{Ic}}^{MZR} \propto f(9(Z - 8.9)) \quad (7)$$

$$P_{\text{IcBL}}^{MZR} \propto f(10(Z - 8.5)) \quad (8)$$

where Z is the metallicity of the galaxy measured as $\log_{10}(12+O/H)$ and estimated using the modified Mass-Metallicity Relation (MZR) given by Eq. 2 in Mannucci et al. (2010) (galaxy metallicity is not included in the CosmoDC2 catalogue). The functions f roughly reproduce both the probability density functions and the cumulative distributions of these hosts shown in Fig. 5 of Modjaz et al. (2020).

We note that the SN Ic/Ic-BL distinction is the only pair of classes that are distinguishable solely by host properties. This provides a unique opportunity to test the value of host galaxy information in distinguishing photometrically-similar transient events.

6.5 Type I Superluminous Supernovae (SLSNe-I)

Superluminous SNe (SLSNe) are unusually bright explosions that may require exotic explanations (e.g., pair instability or magnetar spin-down; Kozyreva & Blinnikov 2015; Nicholl et al. 2017) to explain how the ejecta attain such high energies. Type-I SLSNe are hydrogen-poor and have been found to occur predominantly in low-mass, metal-poor, and highly star-forming galaxies (Lunnan et al. 2014; Perley et al. 2016; Schulze et al. 2018). We model their rate based on the observations of ~ 50 SLSN-I hosts from Lunnan et al. (2014); Perley et al. (2016); Schulze et al. (2018). All studies report SLSN-I hosts with specific star formation rates greater than 10^{-10} yr^{-1} ; thus, we model the SLSN probability to be exponentially suppressed below this threshold.

Based on the observed distribution of host galaxy masses and star formation rates, we further suppress the probability of events in galaxies that are both massive and highly star-forming:

$$P_{\text{SLSNI}} \propto \begin{cases} e^{(x_s+10)}, & \text{for } x_s < -10, x_M < 10 \text{ and } x_f < -0.5 \\ e^{-(x_M-3)}, & \text{for } x_M > 10 \text{ and } x_f > -0.5 \\ 1 & \text{otherwise} \end{cases} \quad (9)$$

where $x_M = \log_{10}(M_*/M_\odot)$ and $x_f = \log_{10}(\text{SFR}/\text{Gyr}^{-1})$. We normalize these probabilities by eye such that hosts in the ‘otherwise’ category all have an equal probability of being selected, hosts beyond the defined boundaries are increasingly less likely to be selected, and the discontinuity at the boundaries is minimized.

6.6 Using short-duration gamma-ray bursts as a proxy for kilonova correlations

The discovery of gravitational-wave event GW170817, followed by short-duration ($\lesssim 2$ sec) Gamma-Ray Burst (sGRB) GRB170817A a few seconds later and the optical kilonova (KN) AT2017gfo several hours later, confirmed the association of these signals during a likely neutron star - neutron star merger (Abbott et al. 2017a,b). The multi-band photometry of AT2017gfo, an event which took place in the nearby ($z \approx 0.00972$) galaxy NGC 4993, provided direct evidence for compact mergers as a site where r-process elements are forged. Nevertheless, many questions remain. Although the colour of the emission reveals information on the fraction of lanthanides and actinides

produced from the neutron-rich ejecta, more events are needed to understand the relationship between an event’s emission and its precise nucleosynthetic yield. Further, the differences between KNe generated from the merging of a neutron star-black hole system and those originating in a neutron star-neutron star collision remain unknown. Though there have been no observations of KNe from a neutron star-black hole system yet, numerical simulations show differences between these types of KNe (Kawaguchi et al. 2016; Tanaka et al. 2014; Shibata & Hotokezaka 2019; Bulla et al. 2021). The strength of the subsequent electromagnetic signal also encodes information regarding the neutron-star equation of state (Bauswein et al. 2017; Li et al. 2021; Raaijmakers et al. 2021). Because our knowledge of these systems starts and ends at this prototypical event, owing to the large sky localization area with LIGO and the low intrinsic event rate, additional KN discoveries in upcoming surveys would vastly improve our understanding of these systems.

Because our aim is to improve the ability to accurately identify a diversity of KN events in upcoming survey streams, we do not want to limit our KN host-galaxy model solely to galaxies matching the properties of NGC 4993 (the host of AT2017gfo). Indeed, whereas NGC 4993 is a quiescent galaxy (Levan et al. 2017), sGRBs have been discovered in a variety of both star-forming and quiescent systems (Prochaska et al. 2006; Berger 2009). Based on recent evidence that these signatures share a common astrophysical site (Abbott et al. 2017a), for this work we assume that sGRBs and KNe inhabit host galaxies with similar properties. This assumption has the added benefit that GRBs are regularly observed across the full sky (D’Avanzo 2015), and as a result we have amassed hundreds of GRB detections to date.

We begin constructing the KN WGTMAP by retrieving the positions of reasonably well-localized sGRBs (uncertainty radius $r_e < 0.01^\circ$ and $t_{90} \lesssim 2$ s) from the NASA Fermi GBM Burst catalogue (von Kienlin et al. 2020; Gruber et al. 2014; von Kienlin et al. 2014; Narayana Bhat et al. 2016) and from the GRB Host Studies catalogue (Savaglio et al. 2006b). Next, we use the `astro_ghost`¹¹ software to identify the most-likely host galaxy associated with these events and retrieve photometric data from these galaxies. Whereas the original implementation of the package considered only northern-hemisphere galaxies within the Pan-STARRs source catalogue (Flewelling et al. 2020), for this work we have extended the code to query the SkyMapper catalogue (Onken et al. 2019) for southern-hemisphere sources as well. After visually verifying each association, we arrive at a sample of 11 sGRB-hosts, one of which is NGC 4993. Apparent *gri*-band magnitudes are reported for all hosts except two, which lack high-SNR brightness estimates in the *r* band. We then convert apparent magnitudes to absolute magnitudes. We adopt the galaxies’ spectroscopic redshifts as reported in the NASA/IPAC Extragalactic Database¹² where possible, and use a photo-*z* estimator¹³ for the galaxies without a reported redshift. We generate a kernel density estimate (KDE) to approximate the joint distribution of absolute magnitudes in *gri* for these hosts using the available data. From this KDE and using a Gaussian kernel, we determine best-fit bandwidths of 0.93, 0.62, and 0.57 for *gri*-band absolute magnitudes, respectively.

We then sample from this KDE along a uniformly-spaced grid spanning the apparent magnitudes of a random sample of CosmoDC2 galaxies. This sampling forms the basis of our KN WGTMAP.

¹¹ <https://pypi.org/project/astro-ghost/>

¹² <https://ned.ipac.caltech.edu/>

¹³ https://github.com/awe2/easy_photoz/tree/main

To select hosts for our KN simulations, we initially applied this WGTMAP to the HOSTLIB of randomly-sampled cosmoDC2 galaxies. The resulting simulations exhibited an unrealistically small scatter in the host $r - i$ vs. $g - r$ colours. We identified this as a result of tight colour correlations in the HOSTLIB coming from the cosmoDC2 colour assignment, unrelated to the WGTMAP construction. To correct for this artifact, we shift the apparent magnitudes of cosmoDC2 galaxies in each LSST band by a random number less than or equal to the observational uncertainty in that band. This sample of magnitude-shifted cosmoDC2 galaxies is stored as a distinct HOSTLIB and used only for the KN class. The shifts are effective at smearing the tight colour relationship. The KN WGTMAP is unchanged.

6.7 Active Galactic Nuclei

The emission from Active Galactic Nuclei (AGN) originates from black holes at the centers of host galaxies in one of various states of active accretion (Lynden-Bell 1969). Multiple theoretical and observational studies have lent support for the co-evolution of supermassive black-holes and the galaxies they inhabit (Ellison et al. 2011; Rosario et al. 2015), making these bright transients powerful probes both for galaxy formation and black-hole evolution across cosmic time (Alonso et al. 2007). Kauffmann et al. (2003) found by analyzing a sample of 22,623 AGN within $z < 0.3$ that these transients occur predominantly in massive ($> 10^{10} M_{\odot}$) galaxies. The properties of an AGN, including its overall luminosity and the characteristic timescale of its optical variability, have also been linked to the luminosity and stellar mass of its host, respectively (Heckman 1980; Ho et al. 1997; Burke et al. 2021).

To simulate the properties of AGN host galaxies, we define a normally-distributed probability density function with scale factor s and a shift factor c over the logarithm of stellar mass, x_M :

$$P_{\text{AGN}} \propto e^{-((x_M - c)/s)^2/2} \quad (10)$$

We set $c=10.8$ and $s=0.5$ to reproduce the distribution of AGN host galaxies seen in Fig. 5 of Kauffmann et al. (2003).

6.8 Tidal Disruption Events

In a Tidal Disruption Event (TDE), material from a star is stripped during close passage to a supermassive black hole (SMBH; Ayal et al. 2000; Strubbe & Quataert 2009). The stripped material circularizes into a debris disk around the SMBH and accretes onto it, resulting in a luminous flare spanning the electromagnetic spectrum. This occurs when the separation between the star and the SMBH falls within the tidal disruption radius of the star and, in some cases, the star is completely destroyed. Early detection and characterization of these events facilitates photometric and spectroscopic follow-up that illuminates the dynamic accretion physics of SMBHs across a range of mass scales (particularly for quiescent black holes; Evans & Kochanek 1989). To date, however, only a small number of these events have been observed in detail. TDEs are found predominantly in post-starburst galaxies (French et al. 2017, 2020), and these correlations can be incorporated into targeted searches in upcoming surveys (Zabludoff et al. 2021). We encode these correlations into a TDE WGTMAP by constructing the following functional approxima-

tion, which roughly reproduces the distribution of events as a function of host galaxy SFR and M_* as shown in Fig. 3 of French et al. (2020).

$$P(M_*, SFR) \propto \begin{cases} e^{-x_f}, & \text{if } SFR \geq 1 M_{\odot} \text{Gyr}^{-1} \\ & \text{and } M_* < 10^{11} M_{\odot} \\ e^{-x_M}, & \text{if } SFR < 1 M_{\odot} \text{Gyr}^{-1} \\ & \text{and } M_* \geq 10^{11} M_{\odot} \\ e^{-(x_f + x_M)}, & \text{otherwise.} \end{cases} \quad (11)$$

We use the HOSTLIB of randomly-selected cosmoDC2 galaxies for this class.

7 VALIDATION OF HOST GALAXY CORRELATIONS

To validate the SCOTCH catalogue, we first confirm that the correlations described in § 6 appear in the final sample as expected. Fig. 10 displays the SFR vs. M_* relationships for a subset of hosts in six classes. Each matches qualitative trends in host types: SN Ia hosts are massive and highly star-forming, SLSNe-I occur mainly in galaxies with high specific star formation rates (and trace the cosmic star formation rate), and 91 bg-like occur in passive, massive galaxies. The generated samples, which used WGTMAP probabilities from Vincenzi et al. (2021), match the correlations therein, but extend to lower masses and star formation rates due to our use of CosmoDC2 versus their use of observed DES galaxies. To more directly compare the host-galaxy derived properties for each class, we plot the cumulative density functions (CDFs) for M_* and SFR in Fig. 11. The CDFs show that, of all transients simulated in SCOTCH, TDEs are simulated in the lowest-mass host galaxies, followed by SLSNe-I. Simulated AGN are hosted by the highest-mass galaxies, followed by the host galaxies of stripped-envelope systems (particularly SNe Ic). The star formation rate CDFs indicate an overabundance of TDEs and KNe in galaxies of low star formation rate, which agrees with observations of the former in post-starburst galaxies and the latter in NGC 4993, a lenticular galaxy with little ongoing star formation. SNe 91bg-like events in our simulation occur on average in the galaxies with lowest star formation rates, a feature of our exponential suppression in active galaxies for this class. Simulated SNe Iax and SNe Ia occur in galaxies with the highest average star formation rate. For SNe Iax, this reflects the exponential suppression of these events in passive hosts. Although it may seem counter-intuitive that SNe Ia host galaxies are more highly star-forming on average than SNe II, it agrees with the dearth of low-mass SN Ia host galaxies except at the highest star formation rates. Consistent with the fact that we simulated nearly all core-collapse supernovae (besides SNe Ic-BL) with the same WGTMAP and HOSTLIB, the CDFs do not show any clear differences between the host galaxy SFR of different core-collapse sub-classes. The exception is the Ic-BL class, which appears more often in the simulation in galaxies of low mean SFR due to the different implemented WGTMAP. We note that, in our models, we can distinguish between statistical samples of SNe Ic and SNe Ic-BL by the mass of their host galaxy, as SNe Ic-BL occur in lower-metallicity host galaxies (Modjaz et al. 2020) and therefore in lower-mass hosts on average. A detailed analysis of the typical observational uncertainties associated with these derived properties and how they might obfuscate these differences in real data is beyond the scope of this work.

Fig. 12 shows the distributions of host colours within each class. Redder galaxies appear to the upper-right and bluer to the lower-left. We did not directly encode colour correlations into the WGTMAPS

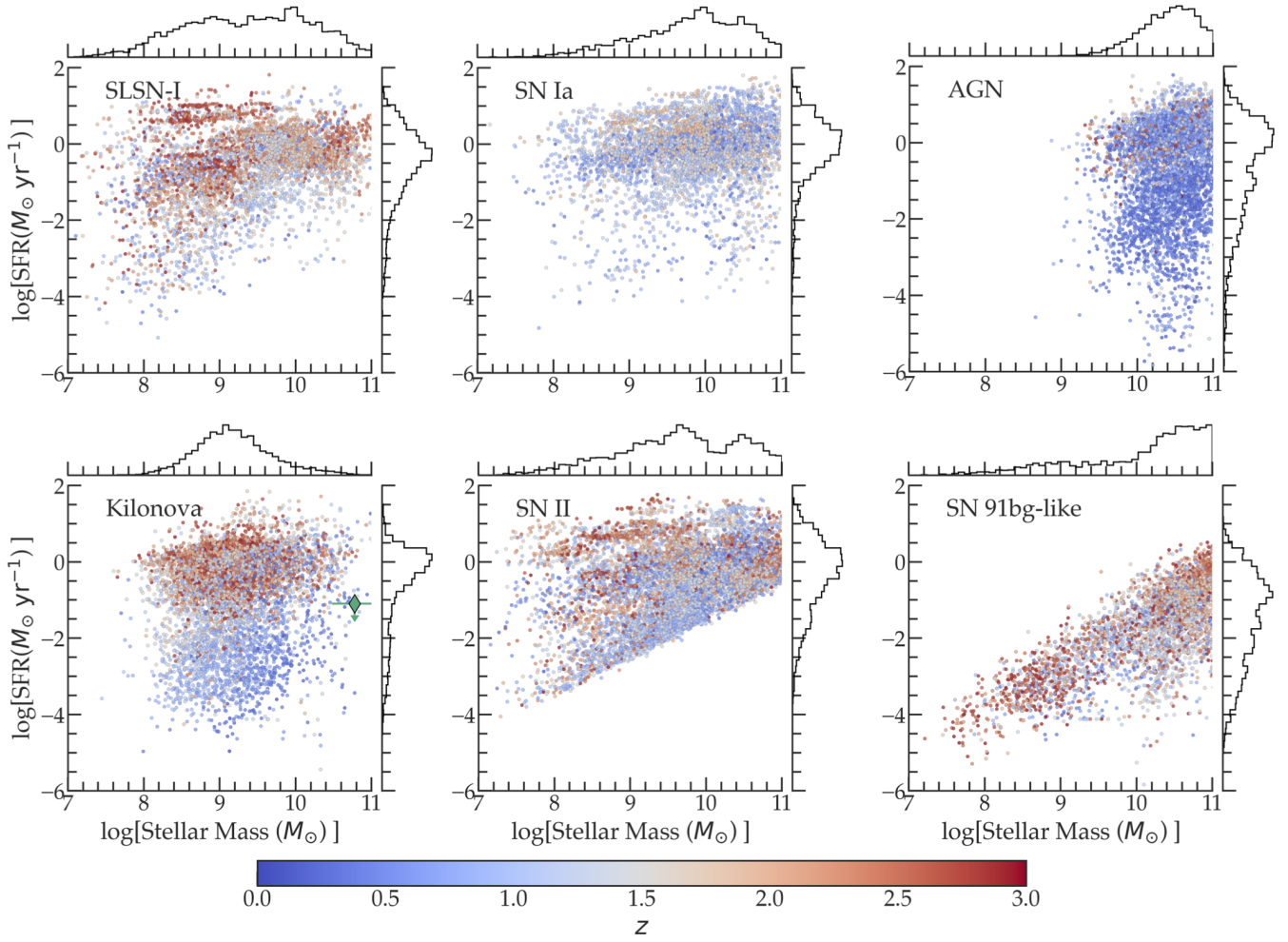


Figure 10. Distribution of derived host-galaxy properties for six simulated classes of transients. Galaxies are coloured by redshift (with red points for high-redshift galaxies). Marginal distributions are given at top and right of each sub-plot. NGC 4993 (the host of GW170817) is shown as the green diamond.

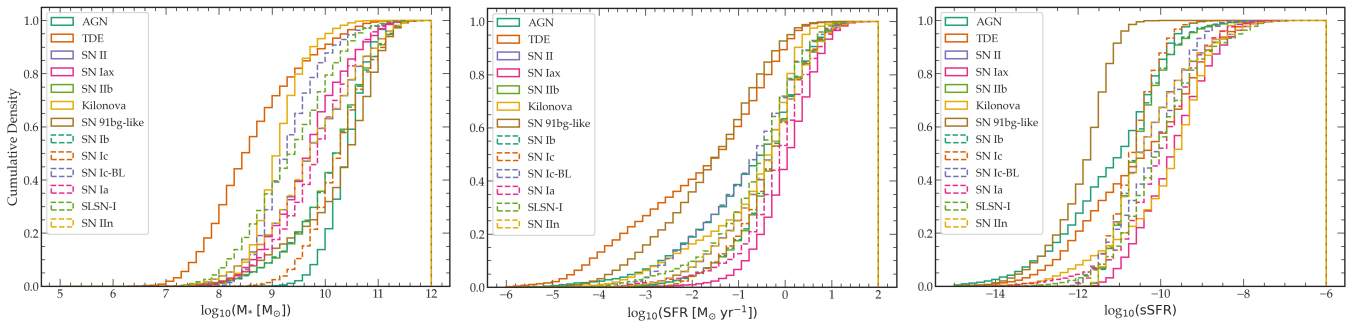


Figure 11. Cumulative density functions (CDFs) in host galaxy stellar mass (left), star formation rate (middle), and specific star formation rate (right) for a representative sample of transient classes in the catalogue. Differences between transient classes reflect a combination of WGTMAP and HOSTLIB effects.

for any of these classes; therefore, the differences between distributions stem from the initial GHOST matching in conjunction with the WGTMAPs in which transient probabilities are dependent on galaxy mass and star formation rate. We caution that we have not converted galaxy colours to the rest-frame for Fig. 12, and so the redshift-dependent rates for each class affect this comparison.

Qualitatively, the observed color plots display many of the intended comparative attributes. Simulated SLSN-I host galaxies are bluer than other SN hosts, reproducing observations that show that these events occur in highly star-forming galaxies (Schulze et al. 2018). SN 91bg-like host galaxies are redder than normal SN Ia, as intended. The KN hosts are surprisingly blue; given the broad

redshift distribution of simulated events (Fig. 5), this may reflect the preference of observed sGRBs for late-type hosts (Fong et al. 2013). As GW170817 (diamond in Fig. 5) occurred in a lenticular galaxy, its host galaxy is redder than the majority of the simulated sample. The simulated $g - r$ distribution for TDE host galaxies is broader than all others, which is consistent with observations (French et al. 2020); however, the $i - z$ span may be unrealistically restricted.

Next, we quantitatively compare the colours of SNe Ia (including peculiar) hosts with the observed distributions reported in Hakobyan et al. (2020, H20). H20 examined $u - r$ colours (SDSS photometry) for a low-redshift sample and found statistically significant differences between the $\langle u - r \rangle$ of ‘normal’ SNe Ia, 91bg-type, and Iax-type host galaxies. The authors reported that galaxies hosting SNe Iax are bluer than normal, while SNe 91bg are redder than normal, with $\Delta\langle u - r \rangle \sim 0.4$ in each case. To investigate this trend in our own data, we calculate the average $u - r$ SDSS rest-frame colour among 10,000 random members of the SCOTCH host sample for the same three classes. Although H20 examined hosts with $z < 0.04$, for the comparison we draw the SCOTCH host sample from the entire $z < 3$ redshift range because our simulation methodology treats high- z host selection equivalently to low- z . The results are shown in Table 3. Our average mean simulated host colour values are significantly bluer than those of the H20 sample for two of the three classes. Our mean SN Iax host colour is also bluer, but consistent within 2σ with the H20 observations. The blue trend may be a consequence of unrealistic galaxy colours in CosmoDC2, as demonstrated in Fig. 3 of Kovacs et al. (2021): the CosmoDC2 $u - g$ distribution is significantly bluer than observational data while $g - r$ is consistent with observations, suggesting that $u - r$ tends to be nonphysically blue. The colour differences between the Ia classes in SCOTCH are in the same direction as the observed differences and are statistically significant. The magnitudes of the differences are somewhat mismatched from observations. Although qualitatively imperfect, the fact that SCOTCH reproduces the general trend in colour differences between the SN Ia sub-types should enable catalogue users to test algorithms which include host information for classification.

We also aim to reproduce observed correlations between the photometric light curves of SNe Ia and their host galaxies. These have been extensively studied in the literature due to the use of these events as cosmological distance indicators. We present the SALT2 (Guy et al. 2007b) fitted parameters x_1 and c (describing the stretch and colour of an SN Ia light curve, respectively) as a function of the intrinsic properties of our associated hosts in Fig. 13. We find similar distributions to those presented in Childress et al. (2013), including a mass-step at $10^{10} M_{\odot}$ (this has been explicitly encoded in our simulations, so its presence is not surprising), and weak anti-correlations between x_1 and both host galaxy M_* and sSFR. We observe a few SALT2 c values above $c=0.2$, and multiple are identified in Childress et al. (2013); although these are anomalous, our model their presence indicates that our correlation model is able to reproduce both the central distribution and the tails of the observed data.

We present $ugrizY$ -band histograms of the absolute magnitudes of host galaxies associated with each transient in Fig. 14. The impact of our encoded correlations is readily apparent by the variation in median and skew between distributions. However, we caution that these histograms mask two important redshift-dependent effects within SCOTCH: the intrinsic rate of different transients across cosmological distances and the $r < 28$ magnitude cut imposed prior to matching in order to cross-match with the 5-yr DC2 image catalogue. The confluence of these effects results in a Malmquist-like bias in the sample, with the distribution of host galaxies for a given class tending toward intrinsically brighter galaxies with increasing redshift (fainter hosts

being unavailable to draw from the HOSTLIBs at those redshifts). For events occurring in galaxies ranging in brightness and observed only at low and intermediate redshifts (e.g., TDEs), we observe a realistic skew toward fainter galaxies that dominate the HOSTLIBs at these redshifts. For bright classes (e.g., SLSNe-I) and common ones spanning the full simulated redshift range (SNe II), the majority of events will be simulated at high-redshift where this bias is strongest. As a result, the histograms in Fig. 14 reveal a distribution for SNe Ia, SNe II, and SLSNe-I skewed toward bright hosts. This skew is stronger in our sample than in observed catalogues (e.g., GHOST), which do not extend this high in redshift; thus we do not plot observed data for comparison in Fig. 14.

We next compare the distributions of various properties of our final sample back to GHOST to examine the combined effects of our two-step host selection process. Fig. 15 shows the galaxy colour distribution for the Hydrogen-poor event HOSTLIB (consisting of SN Ib, Ic, Iib, and SLSN host matches to GHOST) and the distribution of hosts selected by SNANA after WGTMAPS are applied. The WGTMAPS cause the overall $g - r$ distribution to become slightly bluer and more peaked than the GHOST data. Examining the colours for individual host classes reveals how the different WGTMAPS cause the distributions to stratify. The final SLSN-I host sample is bluer than the others, as encoded via SFR. The Ic hosts separate from the Ic-BL hosts in colour space due to the implemented metallicity dependence. Overall, the final combined host grouping remains similar to observed data but the individual host classes within that group are subtly different, demonstrating the combined power of the HOSTLIB + WGTMAP formalism.

To further demonstrate the utility of including both a HOSTLIB and WGTMAP in our simulation, we compare our final results for SN Ia host galaxies with (1) a sample simulated *only* using the GHOST-matched HOSTLIB and no WGTMAP, and (2) a sample simulated using a randomly-selected (unmatched) CosmoDC2 HOSTLIB and the SN Ia WGTMAP. Figure 16 demonstrates how the implementation of either a HOSTLIB *or* a WGTMAP results in reasonable distributions for some, but not other, host properties. Implementing both the HOSTLIB and WGTMAP leads to an improved match with data from both DES (Smith et al. 2020) and GHOST in multi-dimensional parameter space.

8 CATALOGUE ACCESS AND INTENDED USE

The SCOTCH catalogues are presented in HDF5 format and can be accessed at <https://zenodo.org/record/6601211#.Ypj46pDMLhM>. There are two separate catalogues, one for transients and one for hosts, which can be cross-matched to access the complete associated host-transient information. The properties of the transient and host catalogue are listed in Tables 4 and 5, respectively. Each transient in the catalogue is assigned a unique transient ID (TID) and each host a unique galaxy ID (GID), which are reported in both catalogues to enable cross-matching. If an event is unassociated using our pipeline, we populate the host properties with filler values (-999 for most properties, and 99 for photometry in each LSST passband).

We additionally provide the original dc2ID of each galaxy in the CosmoDC2 catalogue, so that users can query the CosmoDC2 image simulations¹⁴ for additional properties. For example, although SCOTCH erases the realistic position information of host galaxies

¹⁴ CosmoDC2_v1.1.4_image at <https://data.lsstdesc.org/doc/cosmodc2>.

	H20		This work	
	$\langle u - r \rangle$	Δ -norm	$\langle u - r \rangle$	Δ -norm
SN Ia (normal)	1.86 ± 0.03		1.372 ± 0.005	
SN Iax	1.47 ± 0.10	-0.39 ± 0.10	1.255 ± 0.006	-0.117 ± 0.008
SN Ia-91bg	2.23 ± 0.05	0.37 ± 0.06	1.908 ± 0.003	0.536 ± 0.007

Table 3. A comparison of the mean rest-frame $u - r$ colour of observed SN Ia host galaxies (all $z < 0.04$) in Hakobyan et al. 2020 (H20) with the simulated catalogue (spanning all redshifts) presented in this work. Each reported uncertainty is the standard error of the mean. Δ -norm is the difference between $\langle u - r \rangle$ of the peculiar SN Ia sample and the normal sample. All simulated hosts are bluer than the observed hosts; SN Ia and SN Ia-91bg hosts are significantly bluer while SN Iax are consistent within 2σ . The qualitative relationship between the classes (SN Iax hosts are bluer, SN 91bg-like hosts are redder) is similar.

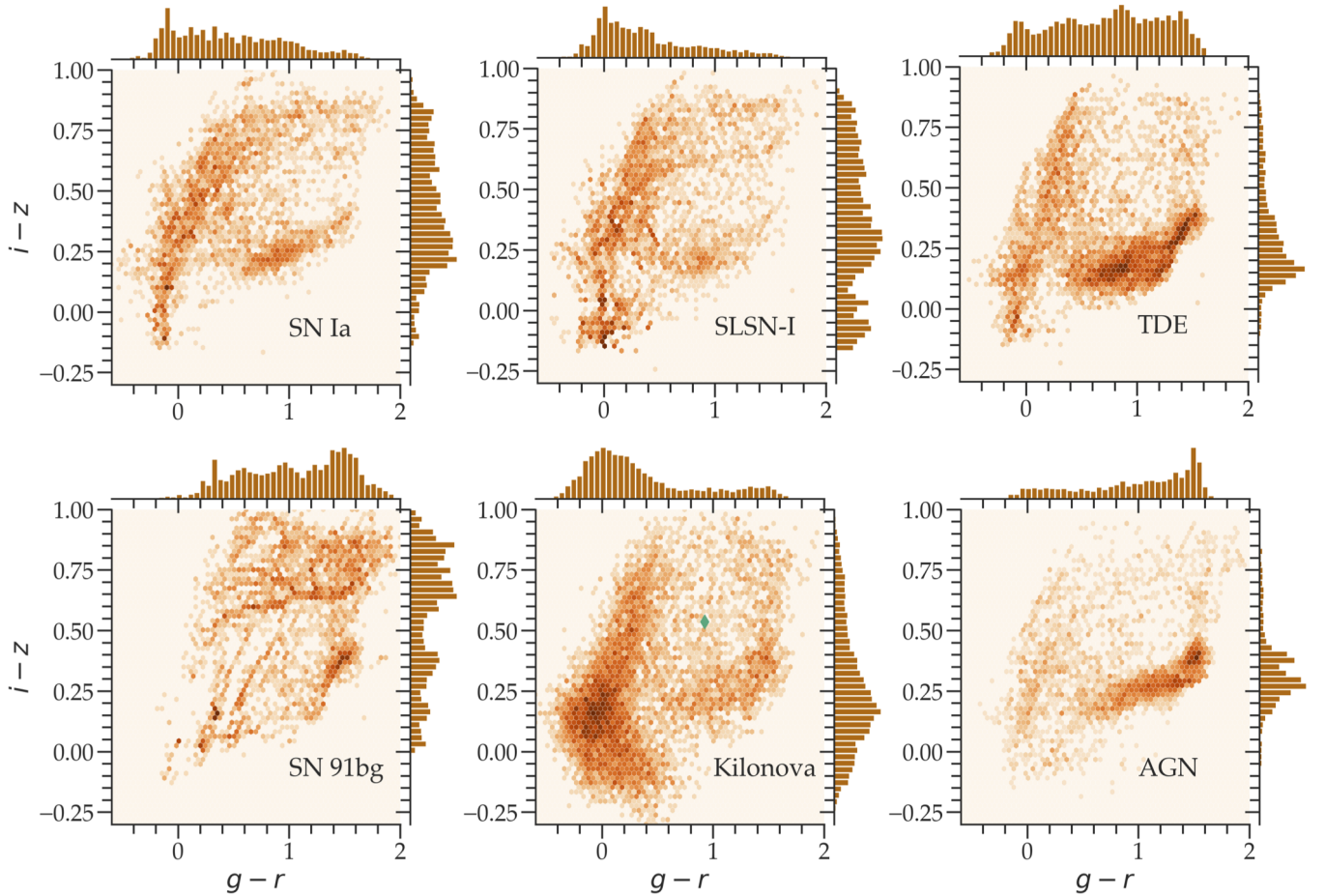


Figure 12. Density distribution of observed colours for simulated transient classes (combining WGTMAP and HOSTLIB contributions). Marginal histograms are shown at top and at right of each sub-panel. The green diamond indicates NGC 4993, the host of the single kilonova observed.

due to the necessary repeat use of HOSTLIB galaxies (see §4), if a user is interested in the original position and large-scale environment of a galaxy, e.g. to check whether the galaxy was a cluster member, they may retrieve the relevant information from CosmoDC2. A user in need of host galaxy SED information may access the original CosmoDC2 SED, find the amount that the galaxy’s redshift has changed from CosmoDC2 to SCOTCH, and red- or blue-shift the SED accordingly. However, we warn that for *kilonova* hosts in particular, the magnitude and colours of SCOTCH hosts are *not* directly traceable to the CosmoDC2 native values, as the kilonovae host magnitudes in SCOTCH have been shifted (§ 6.6).

With top-of-the-galaxy observing conditions, users aiming to simulate optical surveys with similar passbands to LSST have a straight-

forward path to forecasting survey data. The path would include converting the magnitudes accordingly, subselecting events according to expected survey densities, updating transient and host positions to span the survey footprint, and implementing Galactic extinction and atmospheric noise. The ideally-sampled light curves can be degraded by adding noise and by sub-sampling as needed. We provide a series of basic tutorials for querying the catalogue and post-processing the data in Appendix B.

Due to the increased volumes at higher redshifts in the universe and the fact that we simulate a fixed number of transient events per class, the full $z < 3$ catalogue is sparsely populated at very low redshifts. Users wishing to access a larger amount of low- z data may alternatively make use of an additional z -limited catalog that

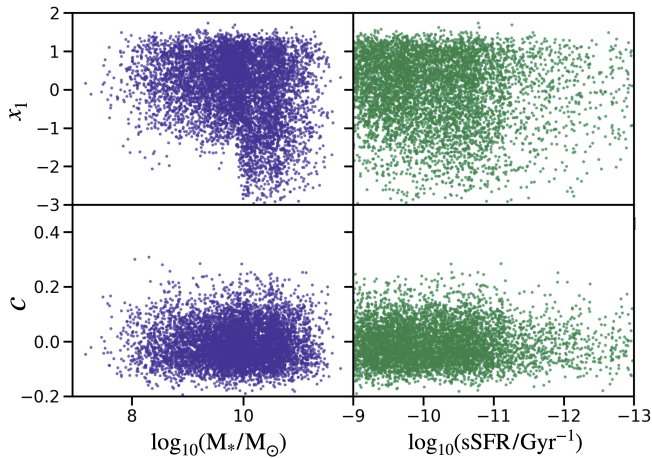


Figure 13. SALT2 (Guy et al. 2007b) fitted parameters x_1 and c as a function of host galaxy M_* and sSFR. Our simulations reproduce the distribution of events observed in Childress et al. (2013).

we release. In this catalog, we restrict the maximum z to 0.8 for each transient class so that the same number of events N , as given in Table 2, are generated at lower redshifts. The $z < 3$ catalogue is named SCOTCH_Z3 and the additional catalogue is named SCOTCH_ZLIM.

For users wishing to simulate significantly different surveys, we also provide the HOSTLIBS and WGTMAPs at <https://zenodo.org/record/6601211#.Ypjd6pDMLhM>.

9 CONCLUSIONS AND DISCUSSION

We have presented our methodology for constructing the SCOTCH catalogue, a dataset consisting of multiple classes of simulated transients and their host galaxies. The final catalogue includes 5 million light curves for 10 distinct classes of supernovae and 3 additional transient classes, as well as the observed and derived properties of their host galaxies and realistic offsets between the galaxy and transient positions. The cadence of these simulated light curves is class-specific in order to resolve rapidly-evolving features while limiting total data volumes. This catalogue significantly advances the framework for simulating the time-domain sky initially constructed for PLASTiCC, which included minimal host-galaxy information.

This catalogue can be used for a broad range of scientific studies. First, teams developing transient classification algorithms for upcoming surveys can test the value of large samples of realistic host information. This added contextual information may help classify transients earlier in their light curves, facilitating rapid follow-up of interesting objects. Host information can also increase the precision of classifications, of particular value for collecting large uncontaminated samples of Type Ia supernovae for precision dark energy measurements. However, users should take caution when training classifiers on this catalogue, as overconfidence in the correlations represented within could limit classifiers from finding transients in hosts that violate conventional wisdom. We have not attempted to include any anomalies in the catalogue to mitigate this problem. Additionally, this catalogue is missing some known transient classes, and does not include any mock new classes of transients. A strong classifier should be able to flag a totally unknown class of event in an upcoming survey.

Beyond classification, this catalogue can be used to forecast future

population-level studies of transients – e.g., for progenitor studies or cosmological applications – using upcoming survey data. Besides the LSST-specific passbands, the catalogue is not tailored to fit the observational limitations of any particular survey. With empirically-derived transient rates extrapolated to $z=3$ and host galaxy magnitudes as faint as $r=28$, users can post-process the catalogue to reflect the expected footprint, depth, and observational biases of planned surveys. The catalogue can then be used to generate a proof-of-concept for science ideas, forecast results, estimate expected biases, and test new methods to mitigate them.

The realism of this simulated catalogue is limited by the assumptions made during the simulation pipeline and the limitations of pre-existing transient-host galaxy catalogues. First, there is limited observational data for many of the transient classes we have simulated. The classes with the least data will have the least accurate host property distributions. We have decided to err on the side of including too-strong correlations reflecting the trends seen in the minimal existing data, so that developers of classification algorithms can learn how to incorporate host galaxy information, even if the correlations are ultimately revealed to be more subtle than extant samples indicate. In the future, data from the Transient Host Exchange (Qin et al. 2022) should be ingested into our simulation framework to consider additional correlations with the classes simulated here as well as correlations with classes not yet simulated. While preparing this manuscript, O’Connor et al. (2022) investigated a series of high-redshift ($z < 2$) sGRB host galaxies and found a potential increase in the number of hostless events with redshift. Given the small number of sGRBs considered in this study, additional work should be devoted to identifying and integrating correlations among high- z samples.

Additionally, we did not attempt to model any evolution with redshift of the host-transient correlations, and therefore host populations at high- z in the catalogue have similar distributions in intrinsic properties to hosts at low- z . Upcoming high- z surveys will shed more light on any potential evolution in host galaxy populations. Finally, the hosts and transients are *not* distributed in a realistic large-scale structure. Although the relative offsets between transients and their host galaxies are realistic, we have avoided placing these systems on the sky so that the catalogue may be of general use for generating synthetic transient catalogues for both northern and southern hemisphere surveys by the user. Therefore, the SCOTCH catalogue cannot be used to forecast cosmological applications of surveys that rely on realistic positions or velocities within the large-scale structure.

Although not the focus of this work, the validated correlations between simulated SNe Ia and their host galaxies are encouraging. Because we have linked the properties of observed SN Ia host galaxies to synthetic galaxies in CosmoDC2, myriad intrinsic host properties are available. Additional work should be done to evaluate the use of synthetic SNe Ia for cosmological analyses, and explore additional correlations between Hubble Residuals and the CosmoDC2 properties of host galaxies.

Multiple improvements could be made to this catalogue. A full-sky simulation could be used rather than the current iteration of CosmoDC2, which would allow the supernovae simulated with SNANA to be shifted to the relative coordinates of their host galaxies. This would maintain realistic large-scale structure and allow for a broader range of uses. Another extension of this work would be to implement correlations between a transient and its location within a galaxy, as multiple studies have revealed local correlations with transient class. For some classes (e.g., TDEs), this local information may be more valuable in early classification than global host galaxy information.

In addition to these catalogue-level corrections, our methods could be expanded to produce simulated images. This is a non-trivial issue

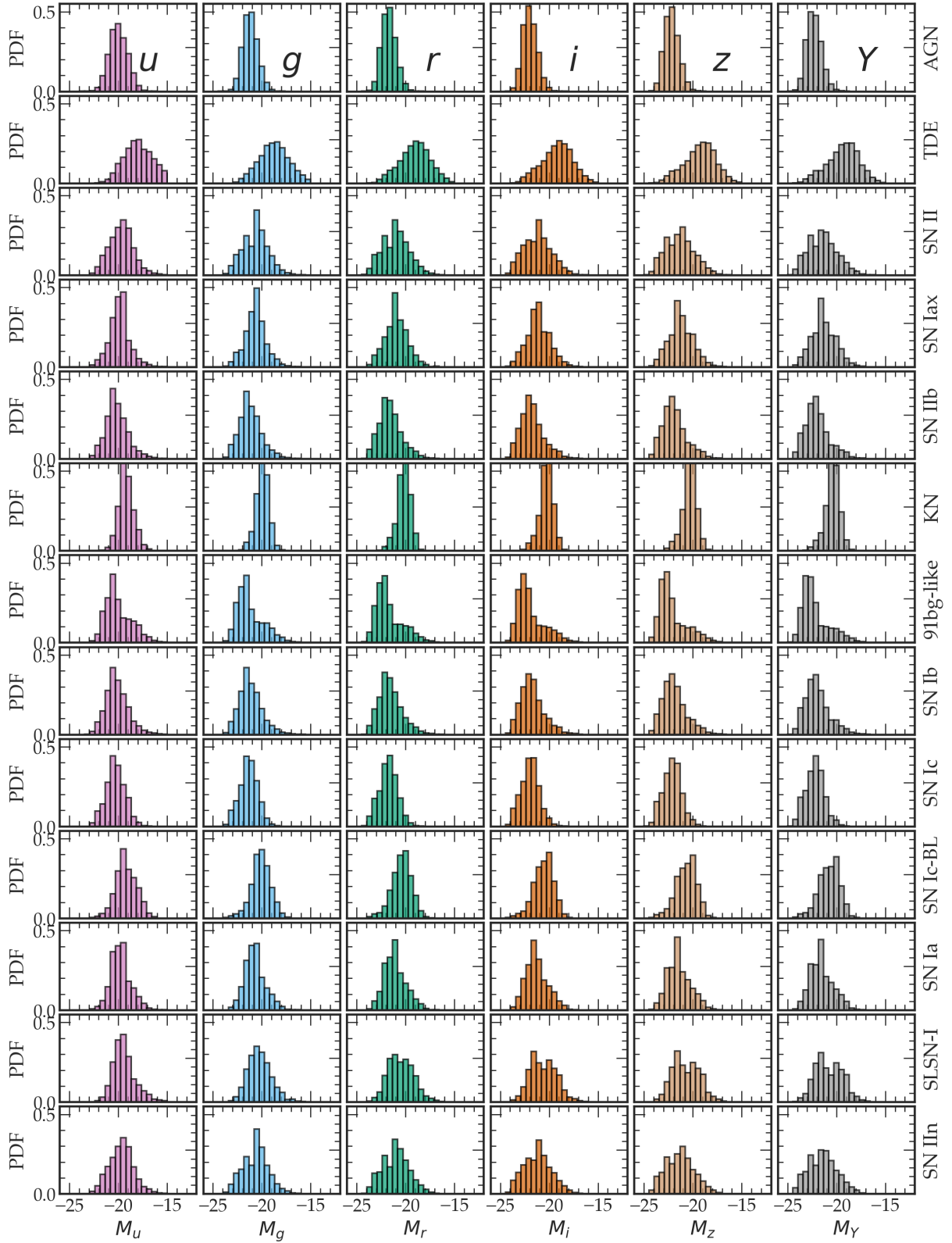


Figure 14. Distribution of host-galaxy absolute magnitudes for a representative sample of simulated transients using both HOSTLIBS and WGTMAPS. Photometry is shown in the LSST filter system.

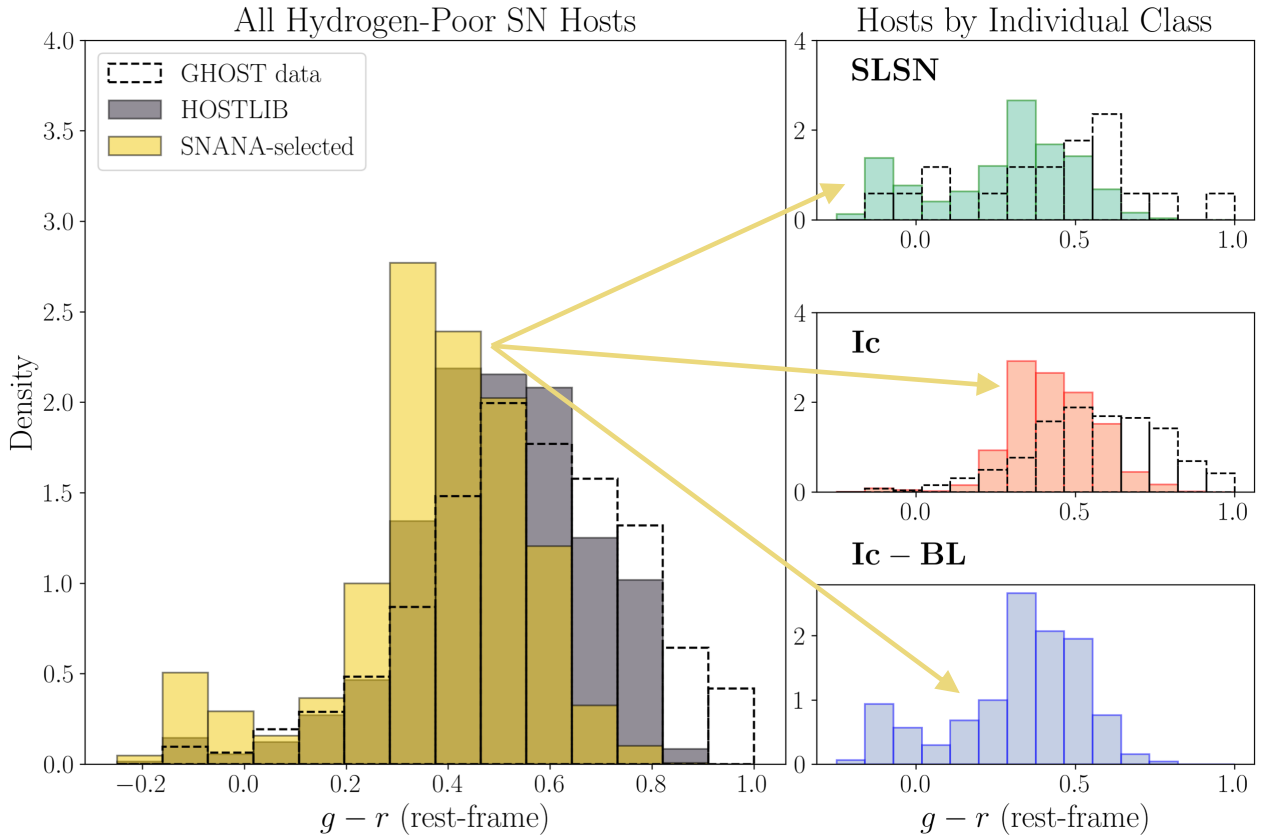


Figure 15. Histogram of $g - r$ colour for synthetic Hydrogen-poor SN hosts before and after running the SNANA simulation. **Left:** The HOSTLIB of all H-poor (Ib/c, SLSN, Iib) hosts (gray), which was tailored to match the GHOST data (dashed line). The hosts selected after running the SNANA simulation for all H-poor classes with their respective WGTMAPs are shown in yellow. **Right:** SNANA-selected hosts of SLSN, Ic, and Ic-BL events. SLSN hosts are bluest, and Ic-BL hosts are bluer than the rest of the Ic class due to SFR and metallicity correlations. GHOST data are shown with a dashed outline, and we avoid plotting SNe Ic-BL hosts in GHOST due to the small sample size.

Variable	Summary
TID	Transient ID
z	True Redshift (of host and transient)
GID	Host-galaxy ID
MJD	Array of Modified Julian Dates of light curve observations (only spacing is meaningful)
$m_{\langle \text{band} \rangle}$	Apparent brightness in LSST <i>ugrizY</i> bands (AB magnitudes)
Class	Transient class
Model	Simulation model from Table 2
Cadence	Time-spacing of light curve samples [days]
RA_{off}	Transient offset from host nucleus in R.A. ["]
δ_{off}	Transient offset from host nucleus in Dec. ["]
Sep	Total great-circle distance between transient and host nucleus ["]

Table 4. Summary of the transient information in the SCOTCH catalogue.

because the transient image must be overlaid on the host galaxy image as well as surrounded by a realistic background which accurately reflects the galaxy density at the location in the simulation. Machine learning-based algorithms such as Generative Adversarial Networks (GAN) have shown significant promise in generating galaxy images that are both survey-specific and realistic (Fussell & Moews 2019; Dia et al. 2020; Buncher et al. 2021, among others), and conditional

networks allow for the integration of model-specific parameters in generated samples (Ravanbakhsh et al. 2016). A generative model conditioned on transient and host galaxy correlations, along with local galaxy density, could be used to rapidly generate realistic images for the systems in the SCOTCH sample. This framework would represent a significant milestone toward complete end-to-end validation of survey infrastructure.

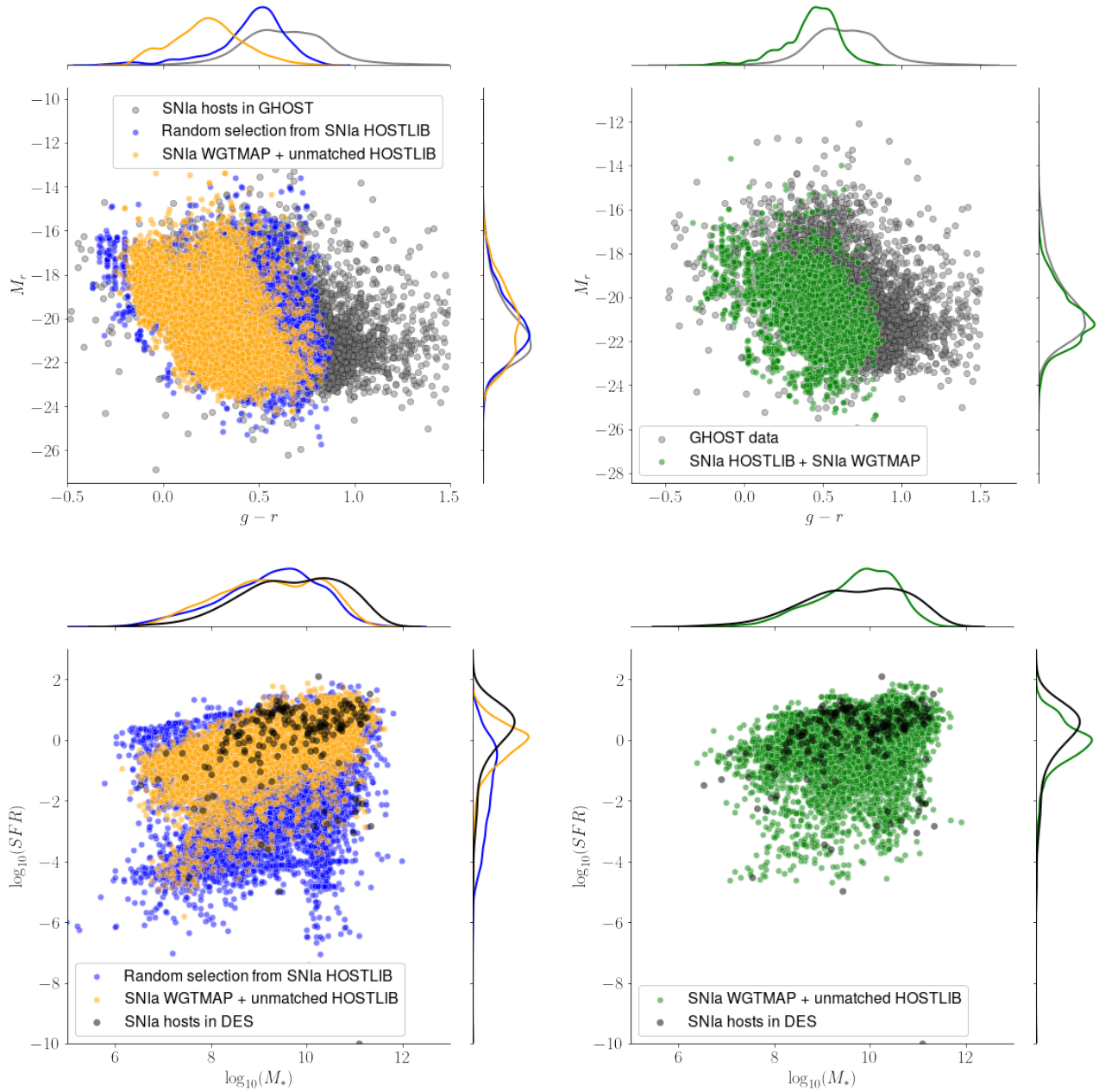


Figure 16. Simulated SN Ia hosts compared to real data for simulations using either a HOSTLIB or a WGTMAP (left), and simulations using both (right). Marginal kernel density estimates are shown at top and at right in each panel. The HOSTLIB-only simulation (blue) decently reproduces the colour-magnitude spread of SN Ia hosts in GHOST (upper left), although less well in $g-r$ than in M_r due to the CosmoDC2 colour limitations. The blue points, however, are a poor match to DES data from [Smith et al. \(2020\)](#) in SFR-stellar mass (SFR- M_*) space (lower left), especially in the SFR distribution. A random sampling of CosmoDC2 galaxies which is associated with SNANA transients via a realistic WGTMAP (yellow) yields more realistic SFR- M_* results but does worse in colour-magnitude space. Notably, the yellow distribution in $g-r$ is in strong disagreement with GHOST. Simulations using both HOSTLIB and WGTMAP (green at right) result in decent matches to both data sets in both parameter spaces.

ACKNOWLEDGEMENTS

This paper has undergone internal review in the LSST Dark Energy Science Collaboration. The internal reviewers were Eve Kovacs, Christopher Frohmaier, Benjamin Rose, and Douglas Clowe. The authors thank the internal reviewers for their thorough reviews of this work, which have improved both its content and presentation.

The DESC acknowledges ongoing support from the Institut Na-

tional de Physique Nucléaire et de Physique des Particules in France; the Science & Technology Facilities Council in the United Kingdom; and the Department of Energy, the National Science Foundation, and the LSST Corporation in the United States. DESC uses resources of the IN2P3 Computing Center (CC-IN2P3–Lyon/Villeurbanne - France) funded by the Centre National de la Recherche Scientifique; the National Energy Research Scientific Computing Center, a DOE Office of Science User Facility supported by the Office of Science

Variable	Summary
GID	Host-galaxy ID
TID	Transient ID
dc2ID	ID of corresponding CosmoDC2 galaxy
$m_{\langle \text{band} \rangle}$	Apparent AB magnitudes in LSST <i>ugrizY</i> bands
$\sigma_{m, \langle \text{band} \rangle}$	10-year estimated apparent AB magnitude errors for LSST
e	Shear ellipticity* $(1 - q)/(1 + q)$, where q is the axis ratio
R_d	Disk half-light radius in physical kpc
R_s	Spheroid half-light radius in physical kpc
$\log(M_*)$	Log stellar mass [M_\odot]
$\log(SFR)$	Log star formation rate [M_\odot/yr]
n_i	Sersic index for $i=[0, 1]$; $n_0=1$ (exponential disk) and $n_1=4$ (deVaucouleurs bulge)
w_i	Weight of $i=[0, 1]$ Sersic components (bulge and disk)
a_i	Major-axis half-light size ["] for $i=[0, 1]$ Sersic components
b_i	Minor-axis half-light size ["] for $i=[0, 1]$ Sersic components
e_i	Ellipticity of $i=[0, 1]$ Sersic components
e_{tot}	Luminosity-weighted sum of bulge and disk ellipticities
a_{rot}	Rotation angle of major axis with respect to the +RA coordinate [°]

Table 5. Summary of the host galaxy information in the SCOTCH catalogue. We note that the original CosmoDC2 catalog contains inaccurate ellipticities due to a bug; in SCOTCH, we report the corrected ellipticity and minor axis values following the corrections from https://github.com/LSSTDESC/gcr-catalogs/blob/ellipticity_bug_fix/GCRCatalogs/cosmodc2.py.

of the U.S. Department of Energy under Contract No. DE-AC02-05CH11231; STFC DiRAC HPC Facilities, funded by UK BIS National E-infrastructure capital grants; and the UK particle physics grid, supported by the GridPP Collaboration. This work was performed in part under DOE Contract DE-AC02-76SF00515.

M.L. acknowledges the support of the Natural Sciences and Engineering Research Council of Canada (NSERC) [PGSD3 - 559296 - 2021]. M.L. also partially conducted this research while supported by the Queen Elizabeth II/Graduate Scholarships in Science and Technology (QEII-GSST).

A.G. is supported by the National Science Foundation Graduate Research Fellowship Program under Grant No. DGE-1746047. A.G. further acknowledges funding from the Center for Astrophysical Surveys Fellowship at UIUC/NCSA and the Illinois Distinguished Fellowship.

The Pan-STARRS1 Surveys (PS1) and the PS1 public science archive have been made possible through contributions by the Institute for Astronomy, the University of Hawaii, the Pan-STARRS Project Office, the Max-Planck Society and its participating institutes, the Max Planck Institute for Astronomy, Heidelberg and the Max Planck Institute for Extraterrestrial Physics, Garching, The Johns Hopkins University, Durham University, the University of Edinburgh, the Queen’s University Belfast, the Harvard-Smithsonian Center for Astrophysics, the Las Cumbres Observatory Global Telescope Network Incorporated, the National Central University of Taiwan, the Space Telescope Science Institute, the National Aeronautics and Space Administration under Grant No. NNX08AR22G issued through the Planetary Science Division of the NASA Science Mission Directorate, the National Science Foundation Grant No. AST-1238877, the University of Maryland, Eotvos Lorand University (ELTE), the Los Alamos National Laboratory, and the Gordon and Betty Moore Foundation.

The Dunlap Institute is funded through an endowment established by the David Dunlap family and the University of Toronto. The authors at the University of Toronto acknowledge that the land on which the University of Toronto is built is the traditional territory of the Haudenosaunee, and most recently, the territory of the Mississaugas of the New Credit First Nation. R.H is a CIFAR Azrieli

Global Scholar in the Gravity and the Extreme Universe Program, and acknowledges funding from the Alfred P. Sloan Foundation, the National Science and Engineering Research Council of Canada and the Connaught Fund. This research made use of the “K-corrections calculator” service available at <http://kcor.sai.msu.ru/>.

This work was partially enabled by funding from the UCL Cosmoparticle Initiative.

L.S. is supported by the Data Science in Multi-Messenger Astrophysics program at the University of Minnesota.

J.F.C. is supported by the U.S. Department of Energy, Office of Science, under Award DE-SC0011665.

A.I.M. acknowledges support from the Max Planck Society and the Alexander von Humboldt Foundation in the framework of the Max Planck-Humboldt Research Award endowed by the Federal Ministry of Education and Research.

This project uses models developed for the Photometric LSST Astronomical Time-series Classification Challenge. PLAsTiCC was a joint project between the Dark Energy Science Collaboration and Transient and Variable Stars Science Collaboration, and was supported by a LSST Enabling Science Grant, as well as funding from Kaggle, a subsidiary of Google.

This research has made use of the GHostS database (www.grbhosts.org), which is partly funded by Spitzer/NASA grant RSA Agreement No. 1287913.

Author contributions are listed below.

M. Lokken: Data curation, SCOTCH simulations and validation, writing - editing, tutorial creation

A. Gagliano: Data curation, SCOTCH simulations and validation, writing - editing, tutorial creation

R. Hložek: supervision, PLAsTiCC data curation and validation, project administration for PLAsTiCC, writing - editing

G. Narayan: supervision, ELAsTiCC data curation and validation, project administration for ELAsTiCC, writing - editing

R. Kessler: supervision, updating code for SNANA simulations, setting up SNANA simulations, writing - editing

J. F. Crenshaw: Supervising use of PZFlow, writing - editing

L. Salo: Data curation of kilonova hosts, writing - editing

C. Alves: SNANA simulation setup, writing - editing

D. Chatterjee: Updating kilonova light curve model, writing - editing
 M. Vincenzi: consulting on WGTMAP and HOSTLIB setup, updating core collapse SN light curve model, writing - editing
 A.I. Malz: Discussions and infrastructure for follow-up work

DATA AVAILABILITY

The simulated data are available at <https://zenodo.org/record/6601211#.Ypjd6pDMLhM> (Lokken et al. 2022). All code used for this project is publicly visible at <https://github.com/LSSTDESC/transient-host-sims>. Users are welcome to report any catalog problems or bugs in the code via GitHub Issues or by e-mail to the authors.

REFERENCES

- Abbott B. P., et al., 2017a, *ApJ*, **848**, L12
 Abbott B. P., et al., 2017b, *ApJ*, **848**, L13
 Abbott T. M. C., et al., 2019, *ApJ*, **872**, L30
 Alonso M. S., Lambas D. G., Tissera P., Coldwell G., 2007, *MNRAS*, **375**, 1017
 Alves C. S., Peiris H. V., Lochner M., McEwen J. D., Allam T., Biswas R., 2022, *The Astrophysical Journal Supplement Series*, **258**, 23
 Anderson J. P., James P. A., Förster F., González-Gaitán S., Haberman S. M., Hamuy M., Lyman J. D., 2015, *MNRAS*, **448**, 732
 Angus C. R., Levan A. J., Perley D. A., Tanvir N. R., Lyman J. D., Stanway E. R., Fruchter A. S., 2016, *MNRAS*, **458**, 84
 Ayal S., Livio M., Piran T., 2000, *ApJ*, **545**, 772
 Barkhudaryan L. V., Hakobyan A. A., Karapetyan A. G., Mamon G. A., Kunth D., Adibekyan V., Turatto M., 2019, *MNRAS*, **490**, 718
 Bauswein A., Just O., Janka H.-T., Stergioulas N., 2017, *ApJ*, **850**, L34
 Bellm E. C., et al., 2019, *PASP*, **131**, 018002
 Berger E., 2009, *ApJ*, **690**, 231
 Betoule M., et al., 2014, *A&A*, **568**, A22
 Blanton M. R., et al., 2017, *AJ*, **154**, 28
 Brout D., Scolnic D., 2021, *ApJ*, **909**, 26
 Brout D., et al., 2019, *ApJ*, **874**, 150
 Bulla M., 2019, *MNRAS*, **489**, 5037
 Bulla M., et al., 2021, *MNRAS*, **501**, 1891
 Buncher B., Sharma A. N., Carrasco Kind M., 2021, *MNRAS*, **503**, 777
 Burke C. J., et al., 2021, *Science*, **373**, 789
 Chambers K. C., et al., 2016, arXiv e-prints, p. arXiv:1612.05560
 Charikar M. S., 2002, in Proceedings of the thirty-fourth annual ACM symposium on Theory of computing. pp 380–388
 Chatterjee D., Narayan G., Aleo P. D., Malanchev K., Muthukrishna D., 2021, *Monthly Notices of the Royal Astronomical Society*, **509**, 914–930
 Childress M., et al., 2013, *ApJ*, **770**, 107
 Chilingarian I. V., Zlotukhin I. A., 2012, *MNRAS*, **419**, 1727
 Chilingarian I. V., Melchior A.-L., Zlotukhin I. Y., 2010, *MNRAS*, **405**, 1409
 Crenshaw J. F., Connolly A., Kalmbach B., 2021, in American Astronomical Society Meeting Abstracts. p. 230.01
 D’Avanzo P., 2015, *Journal of High Energy Astrophysics*, **7**, 73
 Datar M., Immorlica N., Indyk P., Mirrokni V. S., 2004, in Proceedings of the twentieth annual symposium on Computational geometry. pp 253–262
 Dia M., Savary E., Melchior M., Courbin F., 2020, in Pizzo R., Deul E. R., Mol J. D., de Plaa J., Verkouter H., eds, Astronomical Society of the Pacific Conference Series Vol. 527, Astronomical Data Analysis Software and Systems XXIX. p. 175 (arXiv:1909.12160)
 Drout M. R., et al., 2014, *ApJ*, **794**, 23
 Durkan C., Bekasov A., Murray I., Papamakarios G., 2019, in Wallach H. M., Larochelle H., Beygelzimer A., d’Alché-Buc F., Fox E. B., Garnett R., eds, Advances in Neural Information Processing Systems 32. Curran Associates, Inc., Vancouver, Canada, pp 7511–7522 (arXiv:1906.04032)
 Ellison S. L., Patton D. R., Mendel J. T., Scudder J. M., 2011, *MNRAS*, **418**, 2043
 Evans C. R., Kochanek C. S., 1989, *ApJ*, **346**, L13
 Filippenko A. V., et al., 1992, *AJ*, **104**, 1543
 Flewelling H. A., et al., 2020, *ApJS*, **251**, 7
 Foley R. J., Mandel K., 2013, *ApJ*, **778**, 167
 Foley R. J., et al., 2013, *ApJ*, **767**, 57
 Fong W., et al., 2013, *ApJ*, **769**, 56
 French K. D., Arcavi I., Zabludoff A., 2017, *ApJ*, **835**, 176
 French K. D., Wevers T., Law-Smith J., Graur O., Zabludoff A. I., 2020, *Space Sci. Rev.*, **216**, 32
 Fruchter A. S., et al., 2006, *Nature*, **441**, 463
 Fussell L., Moews B., 2019, *MNRAS*, **485**, 3203
 Gagliano A., Narayan G., Engel A., Carrasco Kind M., LSST Dark Energy Science Collaboration 2021, *ApJ*, **908**, 170
 Gaia Collaboration et al., 2016, *A&A*, **595**, A1
 Gardner J. P., et al., 2006, *Space Sci. Rev.*, **123**, 485
 Górski K. M., Hivon E., Banday A. J., Wandelt B. D., Hansen F. K., Reinecke M., Bartelmann M., 2005, *ApJ*, **622**, 759
 Graham J. F., Fruchter A. S., 2013, *ApJ*, **774**, 119
 Gruber D., et al., 2014, *ApJS*, **211**, 12
 Gupta R. R., et al., 2016, *AJ*, **152**, 154
 Guy J., et al., 2007a, *A&A*, **466**, 11
 Guy J., et al., 2007b, *A&A*, **466**, 11
 Hakobyan A. A., Barkhudaryan L. V., Karapetyan A. G., Gevorgyan M. H., Mamon G. A., Kunth D., Adibekyan V., Turatto M., 2020, *MNRAS*, **499**, 1424
 Heckman T. M., 1980, *A&A*, **500**, 187
 Ho L. C., Filippenko A. V., Sargent W. L. W., 1997, *ApJS*, **112**, 315
 Holoien T. W. S., Marshall P. J., Wechsler R. H., 2017, *AJ*, **153**, 249
 Hounsell R., et al., 2018, *ApJ*, **867**, 23
 Ivezić Ž., et al., 2019, *ApJ*, **873**, 111
 Japelj J., et al., 2016, *A&A*, **590**, A129
 Jha S. W., 2017, Type Iax Supernovae. p. 375, doi:10.1007/978-3-319-21846-5_42
 Jimenez Rezende D., Mohamed S., 2015, arXiv e-prints, p. arXiv:1505.05770
 Jonas J. L., 2009, *Proceedings of the IEEE*, **97**, 1522
 Kasen D., Metzger B., Barnes J., Quataert E., Ramirez-Ruiz E., 2017, *Nature*, **551**, 80–84
 Kauffmann G., et al., 2003, *MNRAS*, **346**, 1055
 Kawaguchi K., Kyutoku K., Shibata M., Tanaka M., 2016, *ApJ*, **825**, 52
 Kelly P. L., Kirshner R. P., 2012, *ApJ*, **759**, 107
 Kenworthy W. D., et al., 2021, *ApJ*, **923**, 265
 Kessler R., et al., 2009, *PASP*, **121**, 1028
 Kessler R., et al., 2013, *ApJ*, **764**, 48
 Kessler R., et al., 2019, *PASP*, **131**, 094501
 Korytov D., et al., 2019, *ApJS*, **245**, 26
 Kovacs E., et al., 2021, arXiv e-prints, p. arXiv:2110.03769
 Kozyreva A., Blinnikov S., 2015, *MNRAS*, **454**, 4357
 LSST Dark Energy Science Collaboration (LSST DESC) et al., 2021, *ApJS*, **253**, 31
 LSST Dark Energy Science Collaboration et al., 2021, arXiv e-prints, p. arXiv:2101.04855
 Lampeitl H., et al., 2010, *ApJ*, **722**, 566
 Leloudas G., et al., 2015, *MNRAS*, **449**, 917
 Levan A. J., et al., 2017, *ApJ*, **848**, L28
 Li A., Miao Z., Han S., Zhang B., 2021, *ApJ*, **913**, 27
 [dataset] Lokken M., et al., 2022, SCOTCH Catalogue and Associated Data Files, doi:10.5281/zenodo.6601211, https://doi.org/10.5281/zenodo.6601211
 Lunnan R., et al., 2014, *ApJ*, **787**, 138
 Lynden-Bell D., 1969, *Nature*, **223**, 690
 Mannucci F., Cresci G., Maiolino R., Marconi A., Gnerucci A., 2010, *MNRAS*, **408**, 2115
 Mao Y.-Y., et al., 2018, *ApJS*, **234**, 36
 Modjaz M., Liu Y. Q., Bianco F. B., Graur O., 2016, *ApJ*, **832**, 108

Modjaz M., et al., 2020, *ApJ*, 892, 153
 Möller A., de Boissière T., 2020, *MNRAS*, 491, 4277
 Narayana Bhat P., et al., 2016, *ApJS*, 223, 28
 Nicholl M., Guillochon J., Berger E., 2017, *ApJ*, 850, 55
 O'Connor B., et al., 2022, arXiv e-prints, p. arXiv:2204.09059
 Onken C. A., et al., 2019, *Publ. Astron. Soc. Australia*, 36, e033
 Perley D. A., et al., 2016, *ApJ*, 830, 13
 Planck Collaboration et al., 2020, *A&A*, 641, A6
 Prochaska J. X., et al., 2006, *ApJ*, 642, 989
 Pursiainen M., et al., 2018, *MNRAS*, 481, 894
 Qin Y.-J., et al., 2022, *ApJS*, 259, 13
 Qu H., Sako M., Möller A., Doux C., 2021, *AJ*, 162, 67
 Raaijmakers G., et al., 2021, *ApJ*, 918, L29
 Raskin C., Scannapieco E., Rhoads J., Della Valle M., 2008, *ApJ*, 689, 358
 Ravanbakhsh S., Lanusse F., Mandelbaum R., Schneider J., Poczós B., 2016, arXiv e-prints, p. arXiv:1609.05796
 Rosario D. J., et al., 2015, *A&A*, 573, A85
 Rose B. M., Garnavich P. M., Berg M. A., 2019, *ApJ*, 874, 32
 Roy A., 2021, *Galaxies*, 9, 79
 Salvato M., Ilbert O., Hoyle B., 2019, *Nature Astronomy*, 3, 212
 Savaglio S., Glazebrook K., Le Borgne D., 2006a, in Holt S. S., Gehrels N., Nousek J. A., eds, American Institute of Physics Conference Series Vol. 836, Gamma-Ray Bursts in the Swift Era. pp 540–545 (arXiv:astro-ph/0601528), doi:10.1063/1.2207951
 Savaglio S., Glazebrook K., Le Borgne D., 2006b, in Holt S. S., Gehrels N., Nousek J. A., eds, American Institute of Physics Conference Series Vol. 836, Gamma-Ray Bursts in the Swift Era. pp 540–545 (arXiv:astro-ph/0601528), doi:10.1063/1.2207951
 Schulze S., et al., 2018, *MNRAS*, 473, 1258
 Scolnic D. M., et al., 2018, *ApJ*, 859, 101
 Shappee B., et al., 2014, in American Astronomical Society Meeting Abstracts #223. p. 236.03
 Shibata M., Hotokezaka K., 2019, *Annual Review of Nuclear and Particle Science*, 69, 41
 Shivers I., et al., 2017, *PASP*, 129, 054201
 Smartt S. J., et al., 2017, *Nature*, 551, 75
 Smith M., et al., 2012, *ApJ*, 755, 61
 Smith M., et al., 2020, *MNRAS*, 494, 4426
 Spergel D., et al., 2015, arXiv e-prints, p. arXiv:1503.03757
 Strubbe L. E., Quataert E., 2009, *MNRAS*, 400, 2070
 Sullivan M., et al., 2006, *ApJ*, 648, 868
 Sullivan M., et al., 2010, *MNRAS*, 406, 782
 Svensson K. M., Levan A. J., Tanvir N. R., Fruchter A. S., Strolger L. G., 2010, *MNRAS*, 405, 57
 Takaro T., et al., 2020, *MNRAS*, 493, 986
 Tanaka M., Hotokezaka K., Kyutoku K., Wanajo S., Kiuchi K., Sekiguchi Y., Shibata M., 2014, *ApJ*, 780, 31
 Tonry J. L., et al., 2012, *ApJ*, 750, 99
 Villar V. A., et al., 2020, *ApJ*, 905, 94
 Vincenzi M., Sullivan M., Firth R. E., Gutiérrez C. P., Frohmaier C., Smith M., Angus C., Nichol R. C., 2019, *MNRAS*, 489, 5802
 Vincenzi M., et al., 2021, *MNRAS*, 505, 2819
 Wang J., Shen H. T., Song J., Ji J., 2014, arXiv e-prints, p. arXiv:1408.2927
 Wiseman P., et al., 2020, *MNRAS*, 495, 4040
 Wiseman P., et al., 2021, *MNRAS*, 506, 3330
 Zabludoff A., et al., 2021, *Space Sci. Rev.*, 217, 54
 van den Bergh S., Li W., Filippenko A. V., 2005, *PASP*, 117, 773
 von Kienlin A., et al., 2014, *ApJS*, 211, 13
 von Kienlin A., et al., 2020, *ApJ*, 893, 46

APPENDIX A: APPROXIMATE NEAREST-NEIGHBOURS MATCHING OF GHOST AND COSMODC2 GALAXIES WITH ANNOY

In LSH methods, a hashing function h is constructed that maps a high-dimensionality observation to a scalar such that, for any three

observations a , b , and c for which some distance metric s is defined in the original space, the following criterion is met:

$$d(a, b) < d(b, c) \implies h(a, b) < h(b, c) \quad (\text{A1})$$

In this example, the two observations a and b with a small relative distance will retain a small relative distance (high relative similarity) after being mapped to a scalar value. Because $d \neq h$, the nearest neighbours returned by LSH methods may vary from those returned by a brute-force distance calculation between all observations; but the ‘approximate’ solution is achieved in significantly less time.

A multitude of methods exist both for constructing the hashing function h and the distance measure d (see Wang et al. 2014, for additional details). In the random projection method employed by ANNOY, a catalogue of observations is provided and two are selected at random. A maximum-margin hyperplane is then constructed that separates the two observations (Charikar 2002). This process is repeated and a decision tree is constructed with each node in the tree corresponding to a hyperplane. The hashing function encodes the side of each separating hyperplane the observations fall. Similar to random forest algorithms, multiple decision trees are constructed in ANNOY. The nearest-neighbours returned by an observation query to the space are the indexed observations that fall on the same side of all separating hyperplanes in a combination of decision trees.

In contrast with previous implementations of LSH methods, ANNOY decouples the construction of the indexed space and the querying of the space for individual vectors. Because the indexed space can be saved as a static file and then loaded into shared memory, matching can be achieved in parallel to dramatically reduce matching time.

We construct our indexed space from the following properties of 30M galaxies in CosmoDC2: absolute rest-frame r - and i -band magnitudes, $g - r$ and $i - z$ colours, and redshift. We normalize all properties by the StandardScaler algorithm, after which the distribution for each parameter has a mean of 0 and a variance of 1. Finally, we weight the redshift by 5%, enabling a wider distribution of redshifts in the matched sample than the low- z GHOST data. We select the same parameters from observed galaxies within the GHOST catalogue, normalize them, and query the indexed space for k approximate nearest-neighbours in CosmoDC2. For a transient class i , we set $k = 2 \times 10^6 / N_{i, \text{Ghost}}$, where $N_{i, \text{Ghost}}$ is the number of galaxies of class i in the GHOST catalogue. This allows our matched sample to contain $\sim 2\text{M}$ galaxies for each class.

APPENDIX B: USING THE SCOTCH CATALOGUE

We have released the SCOTCH catalogue as an HDF5 file consisting of a transient table and a host galaxy table. We present an overview of the SCOTCH catalogue hierarchy in Fig. B1, and provide Python code for retrieving basic information about transients and host galaxies below. Full tutorials can be found in the repository associated with this release.¹⁵

B1 Properties of Transient Host Galaxies

To load in the SCOTCH catalogue, we use the Python package `h5py`¹⁶:

¹⁵ https://github.com/LSSTDESC/transient-host-sims/blob/main/notebooks/SCOTCH_walkthroughs.ipynb

¹⁶ <https://www.h5py.org/>

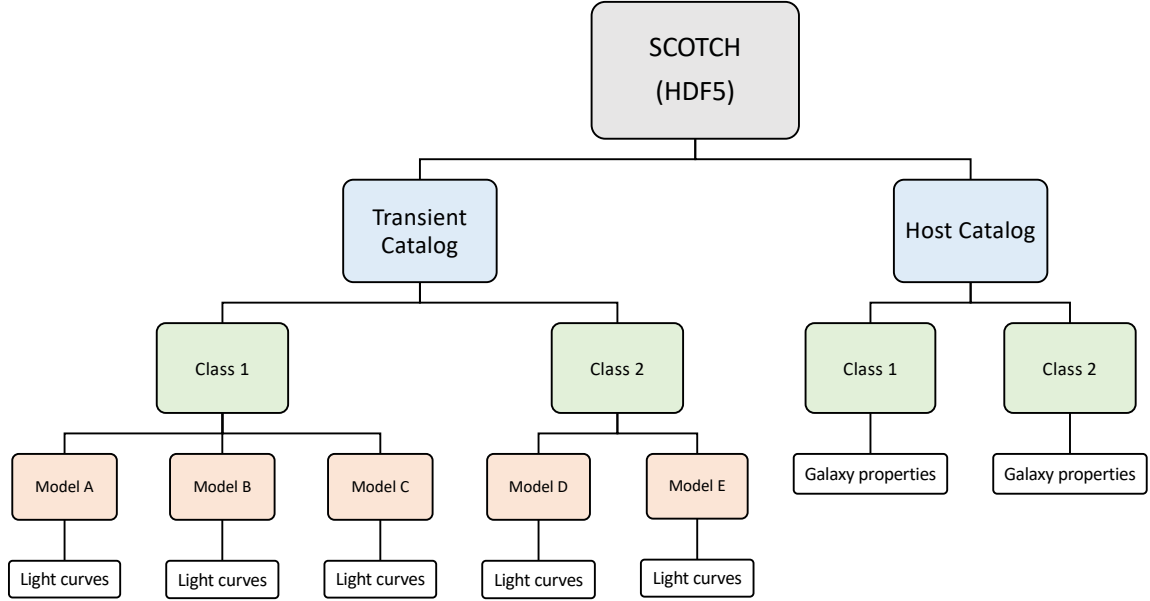


Figure B1. A schematic diagram showing the hierarchical organization of the SCOTCH catalogue. Only two transient classes are shown for illustrative purposes. The Hierarchical Data Format (HDF5) allows users to read only the desired components of the catalogue into memory.

```
>> scotch = h5py.File("./scotch.hdf5", "r")
>> print(scotch.keys())

<KeysViewHDF5 ['HostTable', 'TransientTable']>
```

The host galaxy table is further broken down by transient class:

```
>> scotch_hosts = scotch['HostTable']
>> print(scotch_hosts.keys())

<KeysViewHDF5 ['AGN', 'KN', 'SLSN-I', 'SNII',
'SNIIb', 'SNIa', 'SNIb', 'SNIc', 'TDE']>
```

The parameters linked to each host galaxy are given by retrieving the hosts of a given class:

```
>> print(scotch_hosts['AGN'].keys())

<KeysViewHDF5 ['GID', 'T', 'TID', 'a0', 'a1',
'a_rot', 'b0', 'b1', 'dc2ID', 'ellipticity',
'logMstar', 'logSFR', 'mag_Y', 'mag_g', 'mag_i',
'mag_r', 'mag_u', 'mag_z', 'magerr_Y', 'magerr_g',
'magerr_i', 'magerr_r', 'magerr_u', 'magerr_z',
'n0', 'n1', 'w0', 'w1', 'z']>
```

Values for each parameter can then be retrieved for each event:

```
>> print(scotch_hosts['AGN']['logSFR'][0])

-0.4994781
```

B2 Recovering Transient Light Curves

We now consider the table of transient properties in SCOTCH, and focus on SNe II in the catalogue.

```
>> scotch_transients = scotch['TransientTable']
>> SNII = scotch_transients["SNII"]
```

Each transient table is further broken down by transient model.

```
>> print(SNII.keys())

<KeysViewHDF5 ['SNII+HostXT_V19', 'SNII-NMF',
'SNII-Templates', 'SNIIn+HostXT_V19',
'SNIIn-MOSFIT']>
```

The details for these models are provided in § 4.2 and Kessler et al. (2019).

Below, we retrieve these models and plot the light curves of a single event for each model:

```
>> SNII_models = list(SNII.keys())
>>
>> bands = 'ugrizY'
>> cols_sns = sns.color_palette("colorblind", 10)
>> cols = [cols_sns[4], cols_sns[9], cols_sns[2],
>>         cols_sns[1], 'tab:red', cols_sns[5]]
>>
>> fig, axs = plt.subplots(nrows=3,
>>                          ncols=2, figsize=(10, 10),
>>                          sharex=True, sharey=True)
>> axs[2, 1].set_axis_off()
>> plt.subplots_adjust(hspace=0.25, wspace=0.2)
>>
>> for i in np.arange(len(SNII_models)):
```

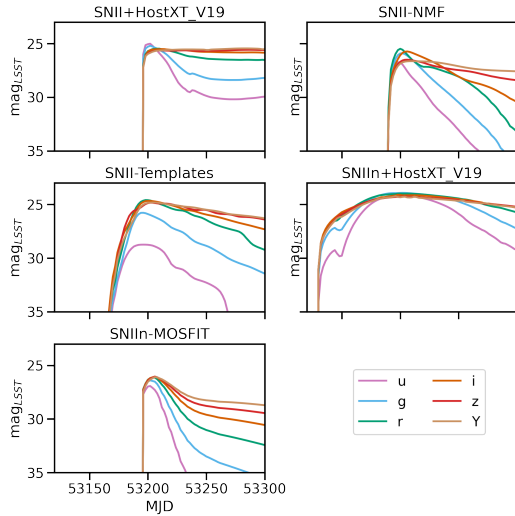


Figure B2. Sample light curves from the SCOTCH catalogue for each SN II model used.

```

>> model = SNII_models[i]
>> SNII_oneModel = SNII[model]
>> ax = axs.ravel()[i]
>> for j in np.arange(len(bands)):
>>     ax.plot(SNII_oneModel['MJD'][0],
>>            SNII_oneModel['mag_%s'
>>            % bands[j]][0],
>>            c=cols[j], label=bands[j])
>> if i==0:
>>     ax.legend(bbox_to_anchor=(2.05, -1.7),
>>              borderaxespad=0, ncol=2)
>> ax.set_ylim((35, 23))
>> ax.set_xlim((53120, 53300))
>> ax.set_ylabel("mag_{LSST}")
>> ax.set_title(model)
>> axs.ravel()[4].set_xlabel("MJD");

```

This code produces Fig. B2.

B3 Survey-Specific Analyses

SCOTCH is intended as a truth catalog, but for many purposes the goal is to simulate observations taken by real surveys with specific footprints and limited efficiency. In the associated tutorials for this work, we provide a basic example of how to emulate observations matching the depths and sky footprint of the LSST Deep Drilling Fields (DDFs), using PLAsTiCC data¹⁷ as a comparison.

We plot the results of our magnitude limit cuts in Fig. B3, where we have also placed SCOTCH SNe realistically on the sky. The redshift distributions for SNe Ia and SLSNe-I now show reasonable agreement to those from the test set of the PLAsTiCC challenge. The remaining discrepancy reflects Milky Way extinction, which is considered in PLAsTiCC and not in SCOTCH; and the difference in how observational limits are incorporated into the SNANA simulated framework (as an efficiency versus SNR curve, and not as an explicit SNR cut as we have imposed here).

The number of objects per class in Table 2 do not represent realistic volumetric rates. However, SNANA provides calculations of the

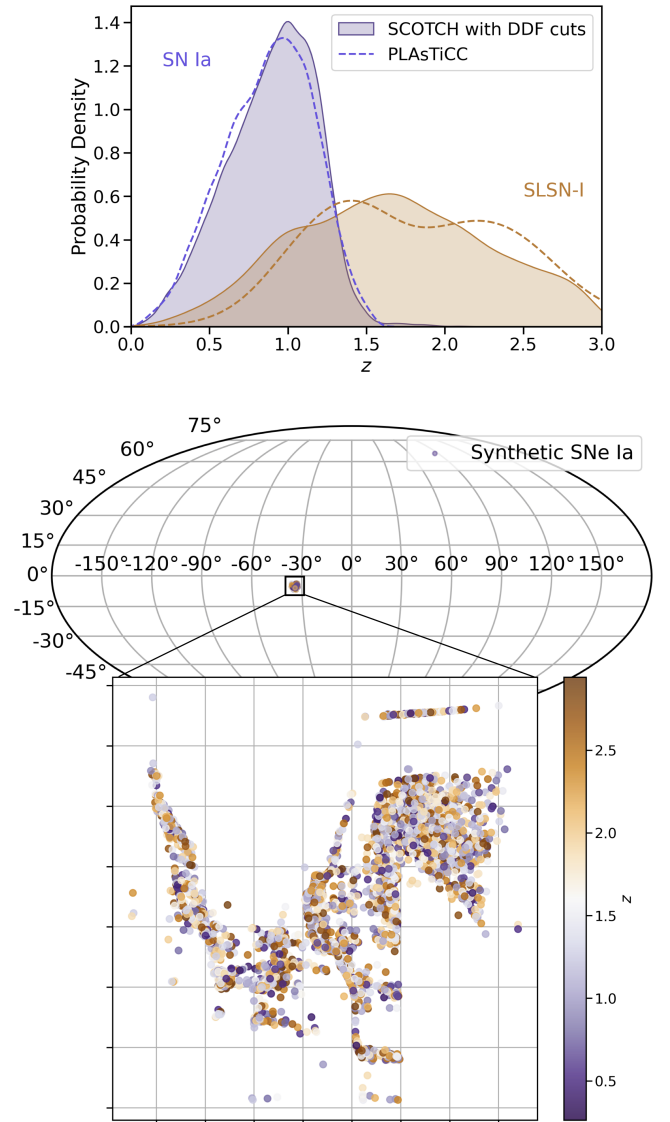


Figure B3. Top: Redshift distributions for SNe simulated within the LSST DDFs. PLAsTiCC data (dashed lines) are compared to SCOTCH SNe after a cut to match the expected 5σ depth of the DDFs. **Bottom:** SCOTCH SNe Ia placed within an LSST DDF field on the sky and colored by redshift. SN Locations were generated by oversampling observations from within a simulated library of DDF observations with PZFlow (Crenshaw et al. 2021). The structure observed for SN locations is not physical, but reflects the limited number of observations used for oversampling. Additional details can be found at the repository for this work.

expected number of events per solid angle per survey time given the input volumetric rates. These are shared in Table B1 to enable re-sampling the simulation to create realistic volumetric populations.

We provide additional tutorials for comparing the properties of transient light curves and their host galaxies in the associated repository.

This paper has been typeset from a $\text{\TeX}/\text{\LaTeX}$ file prepared by the author.

¹⁷ <https://zenodo.org/record/2539456#.YmHSu5LMKNF>

Class	Model name	n [yr ⁻¹]
Ia	SALT2-Ia	21,773,710
	Iax	15,933,345
	91bg-like	5,035,905
Hydrogen-Rich Core-Collapse (2M total)		
SN II	SNII-Templates	15,652,660
	SNII-NMF	15,652,660
	SNII+HostXT_V19	31,402,045
SN IIIn	SNIIIn-MOSFiT	2,270,665
	SNIIIn+HostXT_V19	2,270,665
Stripped Envelope / H-Poor Core-Collapse		
Ib	SNIb-Templates	5,217,675
	SNIb+HostXT_V19	5,217,675
Ic	SNIc-Templates	3,623,355
	SNIc+HostXT_V19	3,623,355
IcBL	SNIcBL+HostXT_V19	1,062,880
IIb	SNIIb+HostXT_V19	10,531,710
SLSN-I	SLSN-I-MOSFiT	53,290
KN	Kasen 2017	122,640
	Bulla 2019	122,640
TDE	TDE_MOSFiT	38,690

Table B1. Number of transients per year, n , for the entire sky and for $z < 3$. The relative amounts of core collapse SNe follow the relative rates measured by [Shivvers et al. \(2017\)](#).